AECL-7773

ATOMIC ENERGY OF CANADA LIMITED

L'ÉNERGIE ATOMIQUE DU CANADA LIMITÉE

NEUTRON AND X-RAY SCATTERING STUDIES FERROELECTRIC PHASE TRANSITIONS

Etude par diffusion des neutrons et des rayons X des transitions de phase ferroélectriques

G. DOLLING

Chalk River Nuclear Laboratories Laboratoires nucléaires de Chalk River

Chalk River, Ontario

August 1982 août

ATOMIC ENERGY OF CANADA LIMITED

Neutron and X-ray Scattering Studies of Ferroelectric Phase Transitions*

G. Dolling

* Three lectures delivered at the University of Sherbrooke Summer School, 1982 May 31 - June 3.

Chalk River Nuclear Laboratories
Chalk River, Ontario, K0J 1J0

August 1982

AECL-7773

L'ENERGIE ATOMIQUE DU CANADA, LIMITEE

Etude par diffusion des neutrons et des rayons X des transitions de phase ferroélectriques*

G. Dolling

Résumé

Le sujet des transitions de phase de type ferroélectrique est abordé au moyen d'exemples de deux catégories importantes (a) transitions de déplacement, p. ex. $KNbO_3$ et (b) transitions ordre-désordre, p. ex. $NaNO_2$. On souligne l'importance de la structure des cristaux et de la dynamique cristalline (c-à-d les relations de dispersion des phonons) pour le comportement ferroélectrique. Les principales méthodes de détermination de la structure sont la diffraction à l'aide de neutrons ou la diffraction de rayons X tandis que la méthode la plus efficace de toutes pour étudier les propriétés des phonons est celle de la diffusion cohérente et inélastique des neutrons. On décrit brièvement la théorie de base de la diffusion par rapport aux lois de la conservation de l'énergie et de la force vive des cristaux. L'application de la théorie de diffusion à la conception des spectromètres neutroniques ainsi que la description générale des propriétés des faisceaux de neutrons thermiques, conduisent à un examen détaillé du type le plus efficace de spectromètre neutronique pour les études de transition de phase, à savoir le spectromètre à cristal à trois axes.

L'histoire de la théorie "soft mode" des transitions de phase en déplacement et son application aux transitions antiferroélectriques et "presque ferroélectriques" dans $SrTiO_3$ constituent une introduction aux plus récents développements réalisés dans ce domaine, y compris les modes mous amortis hypercritiquement, les pics centraux et la diffusion critique, les transitions de phase disproportionnées (p. ex. K_2SeO_4), les amplitudons, les phasons et finalement les solitons. Tout le contenu est descriptif et sert d'introduction aux étudiants diplômés. Une courte bibliographie est annexée pour leur permettre de faire des lectures complémentaires dans le domaine de la diffusion des neutrons et dans celui des transitions de phase.

*Trois cours donnés à l'Ecole d'été de l'Université de Sherbrooke du 31 mai au 3 juin 1982.

Laboratoires nucléaires de Chalk River
Chalk River, Ontario, K0J 1J0

Août 1982

AECL-7773

ATOMIC ENERGY OF CANADA LIMITED

Neutron and X-ray Scattering Studies of Ferroelectric Phase Transitions*

G. Dolling

Abstract

The subject of ferroelectric type phase transitions is introduced by means of examples of two main classes (a) displacive transitions, e.g. $KNbO_3$, and (b) order-disorder transitions, e.g. $NaNO_2$. The significance of crystal structure and crystal dynamics (i.e. the phonon dispersion relations) for ferroelectric behaviour is emphasized. The chief methods for structure determination are X-ray and neutron diffraction, while the most powerful of all techniques for studying phonon properties is that of coherent inelastic neutron scattering. The basic scattering theory underlying these techniques is briefly sketched, with particular reference to the laws of conservation of energy and crystal momentum. Application of the scattering theory to the design of neutron spectrometers, coupled with a general description of the properties of thermal neutron beams, leads to a detailed discussion of the most useful type of neutron spectrometer for phase transition studies, that is, the triple axis crystal spectrometer.

The history of the soft mode theory of displacive phase transitions, and its application to the antiferroelectric and "almost ferroelectric" transitions in $SrTiO_3$, provides an introduction to more recent developments in this area, including overdamped soft modes, central peaks and critical scattering, incommensurate phase transitions (e.g. K_2SeO_4), amplitudons, phasons and finally solitons. The treatment throughout is descriptive and introductory, designed for graduate students. A short bibliography is provided for further reading in the areas of both neutron scattering and phase transitions.

* Three lectures delivered at the University of Sherbrooke Summer School, 1982 May 31 - June 3.

Chalk River Nuclear Laboratories
Chalk River, Ontario, K0J 1J0

August 1982

AECL-7773

Neutron and X-ray Scattering Studies of Ferroelectric Phase Transitions

G. Dolling

Atomic Energy of Canada Research Company

Chalk River Nuclear Laboratories

Chalk River, Ontario, K0J 1J0

1. Structures, Normal Modes and Phase Transitions.

The essential feature of a ferroelectric crystal is that it can exhibit a net electric dipole moment even in the absence of any applied electric field: the centre of positive charge does not coincide with the centre of negative charge. We may imagine a simple diatomic crystal AB containing equal numbers of positive A ions and negative B ions arranged in a symmetrical manner, as in Fig. 1(a). AB is a normal paraelectric crystal. If all the B ions are shifted left by an amount δ, as in Fig. 1(b), we obtain a ferroelectric phase of AB. The dipole moment of each unit cell of the crystal is the same. A more complicated situation may occur in which the B ions in adjacent cells are displaced in equal but opposite directions, Fig. 1(c). The net dipole moment of the whole crystal is clearly zero, and the crystal is said to be antiferroelectric. More general situations may occur in which, for example, the dipole moment in each unit cell

varies sinusoidally from cell to cell with a wavelength which may or may not be commensurate with the crystal lattice constant.

There are many examples of materials which are paraelectric at high temperatures and undergo a series of phase transitions as they are cooled down. Potassium niobate, KNbO3, exhibits three such transitions. As shown in Fig. 2, it is cubic (O_h^1, Pm3m) above 708 K, then tetragonal (C_{4v}^1, P4mm), orthorhombic (C_{2v}^{14}, Amm 2) and finally rhombohedral (C_{3v}^1, P3m1), with transition temperatures 488 K and 223 K, respectively. The lowest three phases are all ferroelectric. Sodium nitrite, $NaNO_2$, is orthorhombic (D_{2h}^{25}, Immm) in its high temperature paraelectric phase above 436 K. Below 434 K, the structure remains orthorhombic (C_{2v}^{20},Im2m), as shown in Fig. 3. The triangular NO_2 groups which carry the dipole moment are all directed along the +b axis, thus leading to a finite net polarization. Above 436 K, there is no net polarization, since the NO_2 groups point along the +b and -b axis with equal probability. In between 434 K and 436 K, one finds a complex sinusoidal phase: in any given bc plane of the crystal, there is a net polarization along the b axis, but its magnitude oscillates sinusoidally as we pass along the a axis from one plane to the next.

These examples clearly indicate the close connection between crystal structure and ferroelectric behaviour, where from now on I will use the term ferroelectric to mean any type of variation of the electric dipole moment per unit cell from one cell to the next even if the net polarization is zero. The two leading methods of determining crystal structure are neutron and X-ray diffraction, and I will devote a part of my lectures to a discussion of these diffraction techniques. When we speak of crystal structure, however, we are dealing with the average positions of the atoms or ions in the crystal - their so-called equilibrium positions. In reality, of course, the ions are always in motion about these equilibrium positions; these motions can be thought of as a superposition of a large number of "lattice waves" or "vibrational modes," of various frequencies and wavelengths. It seems only natural to ask whether there is any connection between structural phase changes and this multitude of vibrational modes. Perhaps the first to ask this question were Raman and Nedungadi, some 42 years ago, in connection with a particular mode of vibration at 220 cm^{-1} of the low temperature α-phase of quartz (SiO_2), and I think it is well worth quoting their final paragraph:-

"The behaviour of the 220 cm^{-1} line clearly indicates that the binding forces which determine the frequency of the corresponding mode of vibration of the crystal lattices diminish

rapidly with rising temperature. It appears therefore reasonable to infer that the increasing excitation of this particular mode of vibration with rising temperature, and the deformation of the atomic arrangement resulting therefrom are in a special measure responsible for the remarkable changes in the properties of the crystal, as well as for inducing the transformation from the α to the β form."

Thus, in addition to determining crystal structures, and their relationship to ferroelectricity, we should also consider whether any of the normal modes of vibration of the crystal may be associated with a ferroelectric phase transition. What kinds of vibrational modes might be expected to be involved in such transitions? With the considerable advantage of hindsight, we would select those modes in which the ions are moving in those directions leading from the non-ferroelectric symmetrical structure towards the positions they would take in the asymmetrical ferroelectric phase. We will discuss the normal mode eigenvectors in more detail later: for the moment I simply want to point out the significance of the wavevector q, that is, 2π times the reciprocal of the wavelength of the normal mode. In a transition to a simple ferroelectric phase, as illustrated in Fig. 1(b), the ionic displacement is the same in every unit cell: the wavelength of this set of displacements can be thought of as either infinite, or as a, or a/2, a/3...a/n, where n is any

integer. The equivalent wavevector ($\underline{q}/2\pi$) is thus 0, 1/a, 2/a, 3/a...n/a. Each of these values represents exactly the same set of ionic displacements, as is illustrated in Fig. 4. In the antiferroelectric example, Fig. 1(c), the wavelength is clearly 2a, or 2a/3, 2a/5, etc., so that ($q/2\pi$) = 0.5/a, 1.5/a, or in general 0.5/a + n/a. The more complicated types of sinusoidally oscillating phases can in the same way be described in terms of modes with appropriate wavevectors $\underline{q}$ related to the sinusoid wavelength.

If we want to study the relationship of normal mode behaviour and these phase transitions, we will in general need to measure the vibration frequencies of modes of many different wavelengths, as a function of temperature, as we approach the phase transition in question. Of the several experimental techniques available for measuring normal mode frequencies, that of coherent neutron inelastic scattering is the most powerful. There are very few restrictions on the types of modes or crystals which can be studied: modes of any wavevector and polarization are readily observable, and there are rather few isotopes (e.g. ^{113}Cd, ^{157}Gd) whose neutron absorption cross sections are so large as to make neutron scattering experiments prohibitively difficult. On the other hand, there are only a few intense sources of thermal neutrons in the world, and the available neutron intensities are quite low relative to the typical photon intensi-

ties available for Raman scattering and infra-red absorption experiments. This means that one usually needs rather large single crystal specimens, typically between 0.1 and 10 cm^3, in order to perform neutron scattering experiments within a reasonable time period.

At this point I would like to insert a short commercial break, to advertise the neutron scattering facilities at Chalk River. The NRU reactor there is by far the best neutron source in Canada, and it ranks about number 4 or 5 in the world. We also have three of the world's very best neutron spectrometers, and a well-established Visitor program whereby scientists from Canada and elsewhere can get their neutron scattering experiments done, usually in collaboration with the local Chalk River staff. End of commercial.

To summarize, then: there are very direct connections between ferroelectric-type phase transitions and both crystal structure and atomic or ionic vibrational modes. To study crystal structure we perform diffraction experiments, with neutron or X-ray beams, while to study atomic vibrations we need a variety of techniques, of which the most powerful is neutron inelastic scattering. The remainder of this lecture will be concerned with the theory behind neutron and X-ray diffraction and neutron inelastic scattering.

2. Scattering Formalism.

A detailed, step-by-step development of the scattering cross section is a rather lengthy and tedious exercise, necessary for complete understanding of the neutron and X-ray scattering business, but not really suitable for treatment in a short lecture series. A bibliography of appropriate references is appended to these notes. Here I confine myself to a few brief remarks about the neutron-nuclear interaction and a summary of the essential steps in the calculation of the cross sections of primary interest.

When a thermal neutron impinges on a solid material, it may either be absorbed or scattered in various ways, or, more usually, it may pass through the solid without change. The cross section for neutron absorption σ_{abs} varies widely from one isotope to another, from 2.4×10^5 barn for ^{157}Gd to less than 2×10^{-4} barn for ^{16}O (1 barn = 10^{-24} cm^2 or 100 fm^2; these values are appropriate for neutrons of energy E = 0.025 eV, corresponding to room temperature. The de Broglie wavelength λ of such a neutron is 1.8 Å*, where $\lambda^2 = h^2/2mE$, h is Planck's constant and m the neutron mass). For almost all isotopes, σ_{abs} is a few barns or less, so that, as mentioned in section 1, absorption usually poses no problem at all for the scattering experiments we are mainly interested in.

The calculation of the scattering cross section proceeds in the following steps:

* 1 Å = 0.1 nm

(a) Since the de Broglie wavelength of a thermal neutron is much greater ($\approx 10^5$ X) than the size of the nucleus, only s-wave scattering from the nucleus is important, and this is isotropic and independent of neutron energy.

(b) The interaction between the neutron and the ith nucleus at position $\underline{r}_i$ is presented by the Fermi pseudo-potential, which is a δ-function:

$$v_i(r) = (2\pi\hbar^2 b_i/m)\ \delta(\underline{r} - \underline{r}_i),$$

where b_i is the so-called bound atom scattering length. The possibility of expressing the potential in this simple form depends upon the assumption that the scattering by a single nucleus is very weak (first Born approximation).

(c) The scattering from the entire assembly of nuclei in the solid is then obtained by summing over the scattering from individual nuclei with due regard to the relative phases of these scattered waves. In general, this will clearly depend on a complicated correlation function describing the relative positions of all nuclei as a function of time. The most important of these functions is the well-known time-dependent pair correction function defined by Van Hove (1954).

(d) The scattering lengths b_i may not be the same for all nuclei of the same element, since different isotopes will scatter differently, and also, if the nuclear spin is non-zero, the scattering amplitude will depend on whether the neutron and

nuclear spins are parallel or antiparallel. Normally, these nuclei having different scattering lengths will be distributed randomly throughout the crystal, and in this case it is convenient to split up the total scattering cross section σ_t into two parts, a coherent (σ_{coh}) and an incoherent (σ_{inc}) part. The precise definitions of these cross sections are given in detail in the references quoted in the bibliography, but the essential points may be understood from the following simple discussion. Let us refer to the very complicated motions of the nuclei in the crystal by a symbolic wave function Ψ. Then the total scattering cross section may be written

$$\sigma_t = \Psi\langle b_i b_j \rangle \qquad (2.1)$$

where $\langle \ldots \rangle$ denotes an average over all pairs of nuclei i, j. If we denote those terms in which i=j by the subscript s (self, or single nucleus) and terms i≠j by subscript d (interference, or distinct nuclei), then

$$\sigma_t = \Psi_s\langle b_i^2 \rangle + \Psi_d\langle b_i \rangle^2 = \Psi_s\{\langle b_i^2 \rangle - \langle b_i \rangle^2\} + \{\Psi_s + \Psi_d\}\langle b_i \rangle^2$$

$$= \sigma_{inc} + \sigma_{coh}. \qquad (2.2)$$

We note that the coherent cross section depends on the square of the mean scattering length, and contains 'interference' and 'self' components of our symbolic wave function. The incoherent cross section, on the other hand, depends only on the scattering from individual nuclei (no interference effects), and is zero if all the b_i are equal. The importance of this division of σ_t

lies in the fact that ψ contains two delta-functions:

$$\delta\{E_o - E_1 \mp \sum_{\ell} h\nu_j(\underline{q}_\ell)\}\ \delta\{\underline{k}_o - \underline{k}_1 - \underline{Q}\}, \qquad (2.3)$$

where

$$\underline{Q} = \sum_{\ell} \underline{q}_\ell + 2\pi\underline{\tau} \ .$$

The summation over ℓ indicates that the scattering process may involve the creation and/or annihilation of ℓ phonons, or quanta of vibrational energy, of wavevectors $\underline{q}_\ell$. $\underline{\tau}$ is any vector of the reciprocal lattice of the crystal, and $\underline{Q}$ is called the momentum transfer vector, since $h\underline{Q}$ is in fact the momentum change suffered by the neutron during the scattering process. $E_o(E_1)$ and $\underline{k}_o(\underline{k}_1)$ are the incident (scattered) neutron energies and wave vectors, respectively ($E_o = h^2|k_o|^2/2m$).

The first delta-function, which expresses conservation of energy, appears in both Ψ_s and Ψ_d, but the second one, conservation of pseudo- or crystal-momentum, appears only in Ψ_d. Thus the incoherent scattering cross section contains no information about the relative positions of different nuclei in the crystal: measurement of σ_{inc} can only give information on the energies or energy distributions of phonons and other excitations in the crystal. Measurements of the coherent scattering, however, can be used to obtain information about the crystal structure and about the phonon dispersion relation $\nu = \nu_j(\underline{q})$. If $\ell = 0$ in eq. (2.3), we have elastic coherent, or Bragg, scattering, for which $E_o = E_1$ and the scattering is confined in

wavevector space to a set of reciprocal lattice points $\underline{\tau}$, from which the crystal structure in real space may be deduced. If $\ell = 1$, we have one-phonon coherent inelastic scattering, which is the scattering process of most interest for studying atomic vibration frequencies. Multiphonon processes ($\ell>2$) are usually to be regarded as a nuisance, contributing unwanted background scattering which makes the observation of the coherent one-phonon scattering more difficult. Of similar nuisance value are all incoherent scattering processes, except in a certain class of experiments, mainly concerned with hydrogenous materials, in which one deliberately measures the incoherent one-phonon scattering. In these experiments, which are possible because the scattering cross section of hydrogen is mainly incoherent, one is interested in measurements of energy levels, or energy distributions; efforts are made to minimize any coherent scattering effects in such cases. I shall not discuss multiphonon or incoherent scattering further.

3. Coherent Elastic Scattering.

After much algebraic manipulation which I shall not reproduce here (see bibliography for details), the differential cross section for coherent elastic scattering of neutrons into solid angle $d\Omega$ from a crystal composed of N unit cells, each containing atoms of type s at position $\underline{r}_s$ with respect to the cell origin, and having coherent scattering lengths b_s, can be expressed in the form

$$\frac{d\sigma}{d\Omega} = N\frac{(2\pi)^3}{V} \sum_{\underline{\tau}} \delta(\underline{Q}-2\pi\underline{\tau}) \left|F(\underline{Q})\right|^2 \qquad (3.1)$$

where the unit cell structure factor is defined by

$$F(\underline{Q}) = \sum_{s} b_s \exp(2\pi i \underline{\tau}\cdot\underline{r}_s) \exp(-W_s) \qquad (3.2)$$

and the Debye-Waller factor W_s by

$$W_s = (h/8\pi N) \sum_{\underline{q}j} (2n_j + 1) \sum_{s} \left|\underline{Q}\cdot\underline{U}_{sj}\right|^2/(m_s \nu_j) \qquad (3.3)$$

The Debye-Waller factor is an average over the atomic displacements from their equilibrium positions $\underline{r}_s$, as represented by the normal mode eigenvectors $\underline{U}_{sj}$. The coherent elastic scattering from a real crystal is actually reduced because the atoms are distributed in a region around their equilibrium positions, to a degree determined by the phonon population factor $n_j = \left[\exp(h\nu_j/k_BT) - 1\right]^{-1}$. As the temperature rises, W_s increases and a larger fraction of $d\sigma/d\Omega$ is diverted into inelastic scattering at the expense of the diffraction peaks at $\underline{Q} = \underline{\tau}$. This latter condition is of course the well-known Bragg Law $n\lambda = 2d \sin\theta$, as illustrated in Fig. 5.

The analogous cross section for the diffraction of X-rays from a crystal is the same as eq. (3.1) except that an additional form factor $f(\underline{Q})$ must be included in the structure factor $F(\underline{Q})$, representing the diffraction pattern from the electron distribution of a single atom. Indeed, a similar form factor is also required for neutron diffraction from crystals containing magnetic ions, which can interact with the neutron magnetic moment. In such cases, the form factor $f(\underline{Q})$ is that for the magnetic

electrons of the ions concerned. There are several interesting examples of crystals, containing magnetic ions, that display both ferroelectric-type and also magnetic phase transitions, but I shall not discuss these magnetic complications further.

Eqs. (3.1) and (3.2) show that the positions of the Bragg peaks in a neutron diffraction pattern can tell us the size of the unit cell of the crystal, while the unit cell structure factor $F(\underline{Q})$ contains information about the disposition of the atoms within one cell. In general there is not sufficient information in these equations to deduce directly and unambiguously the atomic structure from the intensities of the Bragg peaks. The usual procedure is to postulate a set of atomic positions within the unit cell (derived from the Bragg peak positions), and to calculate $F(\underline{Q})$ and hence the peak intensities for comparison with experiment. Refinement of the atomic position parameters by least-squares fitting will then in almost all cases lead to a reliable and well-defined structure.

Crystal structure determination by means of X-ray and neutron diffraction from single crystal and powdered polycrystalline samples is a very wide subject indeed, which would require an entire lecture series on its own. I will spend part of my second lecture on this topic, and again refer you to the bibliography for further information, particularly to Bacon's book.

4. Coherent Inelastic Scattering.

As indicated in the previous section, the existence of the Debye-Waller factor implies that some fraction of the neutrons incident on a crystal is scattered inelastically; the neutron gains or loses energy by annihilating or creating one or more quanta of vibrational energy (phonons) of the crystal. By far the most important of these processes is that involving one phonon, denoted by $\nu_j(\underline{q})$; the expression for this cross section is:

$$\sigma_1(k_o \to k_1)_{coh} = \left[\pi h/M\nu_j(\underline{q})\right](N/V)(k_1/k_o) \times$$

$$\times \left\{n_1(\underline{q}) + 1/2 \pm 1/2\right\}\left|G_j(Q)\right|^2 \Delta_1\Delta_2, \qquad (4.1)$$

where $M = \Sigma_s m_s$, the total mass of one unit cell,

$n_j(q) = (\exp\left[h\nu_j(\underline{q})/k_B T\right] - 1)^{-1}$, the population factor,

$\Delta_1 = \delta(E_o - E_1 \mp h\nu_j(\underline{q})$,

$\Delta_2 = \delta(\underline{k}_o - \underline{k}_1 - \underline{q} - 2\pi\underline{\tau})$,

$$G_j(\underline{Q}) = \underline{Q}\sum_s b_s U_{sj}(\underline{q}) \exp\left[-(2\pi i \underline{\tau}.\underline{r}_s)\right] \exp(-W_s). \qquad (4.2)$$

In these equations, the upper (lower) signs refer to single phonon creation (annihilation), respectively. Equation (4.1) is the cross section for a single phonon mode. To obtain the coherent one-phonon cross section actually measured in an experiment, we must integrate over the range of phonon modes 'observed' by the spectrometer during an experimental scan. This is in general not completely trivial since E_o, $\underline{k}_o$ and $E_1, \underline{k}_1$ are

related. However, for the kind of experimental scan most commonly employed in studies of normal modes and phase transitions, which I will discuss in more detail later, the integration is trivial and the cross section becomes

$$c_1 coh = [Nh/4\pi M\nu_j(\underline{q})](k_1/k_o)[n_j(\underline{q}) + 1/2 \pm 1/2]\left|G_j(\underline{Q})\right|^2 \qquad (4.3)$$

Implicit in this equation are the δ-functions expressing conservation of energy and "crystal" momentum, eqs. (2.3) and (4.1), which are crucial to the success of the coherent inelastic scattering technique for measuring phonon frequencies and eigenvectors. (The term "crystal" momentum merely indicates that the phonon momentum $h\underline{q}$ is arbitrary to the extent of any vector $h\underline{\tau}$ of the reciprocal lattice of the crystal.)

5. Basic Principles.

In order to apply the formalism described in the previous lecture to the determination of crystal structure and phonon frequencies, we require spectrometers which allow us to produce monoenergetic beams of thermal neutrons and to measure their energies after scattering through known angles from single crystal specimens of known orientation.

The energy resolution of a typical neutron scattering measurement is of order 1%. There are at present only two ways of defining thermal neutron energies to this level of precision: (i) by utilizing the phenomenon of coherent elastic (Bragg) scattering of neutrons from selected planes of atoms in a crystal of known lattice spacings, or (ii) by 'chopping' the neutron beam into pulses and then measuring the time of flight of these pulses over a known distance. A wide variety of neutron spectrometers has been constructed over the past decade or so, utilizing methods (i) or (ii) or combination of these. Before discussing these spectrometers in any detail, we briefly enumerate some relevant properties both of Bragg scattering from crystals and of pulsed neutron beams, in order to provide some degree of experimental perspective to those unfamiliar with this subject.

Firstly, let us consider Bragg scattering from a typical crystal, which is governed by the well-known law $\lambda = 2d \sin \theta$,

where d is the spacing or separation between the reflecting planes of atoms, and 2θ is the angle through which the neutron beam is scattered or 'reflected'. Values of d for typical crystal planes range from 0.8 to 3.5 Å, so that a range of angles 2θ from 20° to 160° can be employed to provide neutron wavelengths from about 0.5 to 6 Å. If $2\theta = 60°$, and the angular divergence of the beam (defined by collimation and crystal mosaic spread) is 0.3°, then the wavelength λ will be defined with 0.55% resolution (i.e. 1.1% energy resolution).

Secondly, we consider what characteristics of pulsed neutron beams we would need to achieve the same resolution. Thermal neutrons have a range of velocity $v(v = h/m\lambda)$ between about 500 and 5000 m/s, with a typical velocity being 2000 m/s. In principle, it is possible to obtain arbitrarily high resolution by having very long flight paths, but practical considerations usually place a limit of about 4 m on these path lengths. The typical neutron flight time is thus 2000 μs, and so the neutron pulse length must be no more than 10 μs to achieve 1% energy resolution. There are also limits (2 cm in the above example) on the sample size and detector thickness imposed by the resolution requirements. The presently available methods of producing thermal neutron pulses can readily provide pulses in

the range 5 to 10 μs, but it is extremely difficult to reduce the pulse width significantly below 5 μs. Very high resolution must then be obtained by very long flight paths.

High resolution in crystal spectrometers, on the other hand, is obtained by means of very fine collimation of the neutron beams and by using reflecting crystals of low mosaic spread. In either type of spectrometer, of course, the ultimate limit of resolution is imposed by the necessity to achieve a reasonable count-rate in the detector. In a given experiment, the count-rate varies inversely as a fairly high power (4 or 5) of the overall experimental resolution; this limit, of order 1% energy resolution, is thus set by the neutron fluxes obtainable from present-day neutron sources.

All neutron scattering spectrometers so far constructed operate within a fixed plane, usually horizontal, although a few vertical plane instruments are also in use. By the plane of the spectrometer we mean the plane containing the neutron beams incident upon and scattered from the specimen. Let us define an orthogonal set of axes xyz with x and y defining the plane of the spectrometer. The neutron wave vectors are thus $\underline{k}_o = (k_{ox}, k_{oy}, k_{oz} = 0)$ and $\underline{k}_i = (k_{1x}, k_{1y}, k_{1z} = 0)$, and the energy and momentum conservation equations can be written:

$$(h^2/2m)(k_{ox}^2 + k_{oy}^2 - k_{1x}^2 - k_{1y}^2) = \pm h\nu_j(\underline{q}), \qquad (5.1)$$

$$k_{ox} - k_{1x} = Q_x = 2\pi\tau_x + q_x, \; k_{oy} - k_{1y} = Q_y = 2\pi\tau_y + q_y. \qquad (5.2)$$

The experimental conditions can best be visualized with the help of a reciprocal lattice diagram, Fig. 6, showing the relationship between the neutron wavevectors and the orientation of the crystal specimen. The crystal orientation ψ may be defined by the angle between a selected crystal axis, say y, and the incident neutron beam k_o. The sign convention followed at Chalk River, where the x - y plane is horizontal for all spectrometers, is that + ψ denotes a clockwise rotation of y with respect to k_o, and + Φ implies a clockwise deflection of k_1 with respect to k_o (the observer is assumed to be looking down on the spectrometer). The arrangement in Fig. 6 therefore corresponds to negative values for both ψ and Φ. With this convention, eq. (5.2) can be expressed in terms of the spectrometer angles:

$$Q_x = -|k_o|\sin\psi - |k_1|\sin(\Phi - \psi), \qquad (5.3)$$

$$Q_y = |k_o|\cos\psi - |k_1|\cos(\Phi - \psi). \qquad (5.4)$$

The way in which the magnitudes $|k_o|$ and $|k_1|$ are determined depends on the type of spectrometer, but for the moment we shall assume that they are known. It is clear that we have three relations, eqs. (5.1), (5.3) and (5.4), between four experimental

variables, $|k_0|$, $|k_1|$, Φ and Ψ, so that an additional condition of some sort is necessary to completely specify any experimental point. I will come back to this matter later in this lecture (section 7).

We have now reached a stage at which specific spectrometers and measuring techniques should be discussed. As I mentioned earlier, there are a great many varieties of neutron spectrometer in existence today, each of which has its own advantages and disadvantages, methods of operation, data handling, and so on. If, however, we restrict our attention primarily to studies of phase transitions, crystals structures and specific normal modes, then the most generally useful type of spectrometer is the so-called triple axis crystal spectrometer. We may concentrate our attention on this type of spectrometer, how it works, why it is so useful, and what results have been obtained with its aid. If time permits, I can return later to the subject of other types of spectrometer, describing their advantages and their drawbacks as regards phase transition studies.

6. Crystal Spectrometers.

A schematic diagram of the triple axis crystal spectrometer developed by Brockhouse (1961) is shown in Fig. 7. This venerable old spectrometer has been largely refurbished at Chalk River, and many of the original components have recently been shipped to England to form a historical exhibit at a prestigious international meeting in Cambridge, to commemorate the

50th anniversary of the discovery of the neutron. However, the most modern versions of this spectrometer in use all over the world are essentially the same as this pioneering model, so I can continue to use this ancient diagram to illustrate how all these spectrometers work. The source of thermal neutrons is a section of the heavy water moderator of the NRU reactor, Chalk River. These neutrons, having an approximately maxwellian spectrum of energies, escape through a hole cut in the reactor shielding, and enter a large rotatable shielding drum. A single crystal monochromator, X_1, at the center of this drum, is used to Bragg-reflect neutrons of a particular wavelength and energy through the angle $2\Theta_m$, so that they pass through the collimator C_2 and fall upon the sample S. A low sensitivity monitor detector M2 measures the flux of neutrons incident on the sample, and its counting rate is normally used to control the signal counting times during an experiment. A typical monitor detector consists of a thin layer of natural uranium inside a box with thin aluminum windows. Neutron detection is by means of the ^{235}U fission reaction, and the efficiency is typically $\approx 10^{-4}$, and inversely proportional to the incident neutron wave vector $|k_o|$. The sample sits on a rotatable table whose orientation is denoted by ψ. After scattering from the sample, the neutrons pass through collimator C_3, and those with the appropriate energy may be Bragg-reflected from the analyser crystal X2 into the

signal detector. This detector, together with the analyser crystal, is surrounded by hydrogenous, boron-loaded shielding material of about 9" thickness, to reduce as far as possible the detection of neutrons other than those travelling along the collimated path prescribed above. Hydrogenous shielding material is used, because of the very high scattering cross section of hydrogen, to moderate any fast and epithermal neutrons down to thermal energies, whereupon they may be efficiently absorbed by the ^{10}B isotope of natural boron. ^{6}Li and cadmium are also excellent neutron absorbers, the latter being very widely used as a shielding material in neutron spectroscopy.

The collimators consist of cadmium-plated steel tubes of square cross section (2"x2" inside dimensions), in which a number of cadmium-plated thin steel plates may be mounted, parallel to each other and spaced at regular intervals ('Soller slits').

The BF_3 detector shown here has long since been superseded by the more compact ^{3}He gas detector; this makes use of the (n,p) nuclear reaction, which has a cross section of 5400 barns for 1.8 Å neutrons. Good electrical characteristics can be achieved with up to 10 atm total gas pressure (some krypton is normally mixed with the helium to improve the characteristics). This means that very high efficiency ^{3}He detectors can have much smaller physical dimensions than comparable BF_3 detectors - about the size of a package of cigarettes - so that much less heavy shiel-

ding must be carried by the detector arm which pivots about the analyser crystal X_2. Of course, since we want the detector to receive these neutrons Bragg-reflected from the analyser crystal, the detector arm must always rotate twice the angle through which the analyser rotates.

In order to exploit the full versatility of this type of spectrometer, it is most desirable to be able to drive all four angles $2\theta_m$, $2\theta_a$, ψ and Φ independently, with a precision of the order of 0.01°. Nowadays this control is almost always achieved by means of small on-line computers which perform all the calculations of eqs. (5.1) to (5.4), derive the values for the above four angles at each point on an experimental scan, and drive appropriate stepping motors. Optical encoders mounted on each drive shaft monitor the angular positions and inform the computer when each angle has reached the desired value. Neutron counting is then initiated, for a length of time determined by the number of neutrons passing through the monitor detector just before they strike the sample. Thus every scattered neutron count is automatically normalized to the incident neutron flux, regardless of any variations in source strength or monochromator reflectivity which may occur during the experiment.

7. Constant-Q and Other Types of Scan.

Returning now to eqs. (5.1) - (5.4), which relate the three phonon parameters Q_x, Q_y and ν to the four spectrometer

variables $|k_o|$, $|k_1|$, Φ and Ψ, we can think of several possible ways of performing a neutron scattering experiment. By far the most popular method, that of "Constant-$\underline{Q}$," is the most obvious reason for the enormous success of the triple axis crystal spectrometer in the phase transition studies we are concerned with here. The essential point of this research is that particular values of the wavevector $\underline{Q}$ turn out to be especially significant: all the theoretical interest is concentrated on these particular values, while phonons having other $\underline{Q}$ values play little or no part in the physics of the process. Figure 8(a) shows how to conduct an experiment so that all the neutron scattering results will refer to a particular, pre-selected $\underline{Q}$ value. In this example, I have chosen to fix the scattered neutron wavevector magnitude $|\underline{k}_1|$ throughout the scan. However, $|\underline{k}_o|$, Ψ and Φ are changed in such a way that the neutron wavevector transfer $\underline{Q}$ is always kept fixed at our chosen value - the one of special interest for the phase transition we are studying. The neutron energy transfer is changed, step by step, over a range in which we expect to find the frequency of the phonon corresponding to the fixed $\underline{Q}$ value. The results of such a scan are sketched in Fig. 8(b), on the assumption that the phonon being studied has a rather well-defined frequency. For most points on the scan, the neutron energy transfer is not equal to the phonon energy, and so no coherent one-phonon scattering can occur. When $E_0 - E_1 = h\nu_j(\underline{q})$,

however, both δ-functions in the scattering cross section are satisfied, and we see a sharp peak.

In general, we can program the spectrometer to follow any desired line in $(\underline{Q}, \nu)$ space; such a general scan is illustrated in Fig. 9(a), while Fig. 9(b) shows several possible scanning paths relative to a typical phonon dispersion curve. The value to neutron scattering research of this degree of flexibility and control over the experimental parameters can hardly be overestimated. To attain such control and flexibility in the operation of time-of-flight spectrometers is a much more difficult task.

8. Experimental Difficulties: Spurions and Other Glitches.

The above-mentioned advantages of crystal spectrometers are not without certain concomitant disadvantages. Most if not all of these can be avoided, once we know that they exist, by suitable planning of the experiments, by the use of particular types of monochromating crystals, and by the use of various neutron filters such as polycrystalline Be, single crystal sapphire and pyrolitic graphite. I will discuss here only two of these difficulties by way of illustration; a more detailed account can be found in my article listed in the bibliography.

The first example concerns the fact that Bragg's law $n\lambda = 2d \sin\theta$ permits any integer value n: thus although the analyser crystal of our spectrometer may be set at the angle θ_a to

reflect neutrons of wavelength λ, energy E, it will also in general reflect neutrons of wavelength $\lambda/2$, $\lambda/3$... and energies 4E, 9E... In a hypothetical constant-$\underline{Q}$ experiment, as shown in Fig. 10, we are in effect doing two experiments simultaneously, defined by $\underline{k}_o - \underline{k}_1 = \underline{Q}$ and $\underline{k}_o - 2\underline{k}_1 = \underline{Q}'$, following the locus CC'. It may happen that conservation of energy and crystal momentum are satisfied at some point along the line CC', for a phonon or other excitation of the crystal, completely unrelated to the phonon at the point $\underline{Q}$, and spurious peak will then be observed. A simple way to avoid this is to employ a Ge or Si crystal as analyser, with odd index planes such as (111), since it so happens that the unit cell structure factor, eq. (3.2), for these crystals is identically zero for the n=2 planes, i.e. (222).

The second example is a little more subtle. It may happen that the incident beam $\underline{k}_o$ is Bragg-reflected by the specimen crystal in the direction of the analyser crystal. Of course, the analyser is not set to reflect neutrons of wavevector k_o, but will be a small diffuse scattering intensity of all wavevectors, arising from inelastic and incoherent scattering processes. The intensity finally detected, resulting from two Bragg reflections and one diffuse scattering process, can easily be of the same size as the coherent one-phonon scattering process under investigation. If we suspect that a peak may be due to this, we can easily check it by rotating the analyser a few degrees away from

its reflecting position and repeating the scan. If spurious, the peak will still remain, if genuine, it will disappear. This process and an analogous one in which diffuse scattering of neutrons of wavevector $\underline{k}$ from the monochromator crystal is followed by Bragg reflection at both sample and analyser crystals are illustrated in Fig. 10(b).

There are many little tricks of the trade which can be used to avoid these and other spurious processes and enable the experimenter to ensure the reliability of his results. Indeed, the biggest problem we encounter in all our neutron scattering work does not concern the experiments themselves; obtaining a suitable, large-sized single crystal specimen is often the hardest part of the whole business. We are always on the look-out for people who can grow crystals.

9. Historical Perspective; Examples of Soft Modes.

It seems that the basic idea connecting a vibrational mode tending to zero frequency with the onset of a structural phase transition had occurred independently to at least six different people before 1960, beginning with Raman in 1940, and including Ginzburg in 1949, Frohlich in 1949 and Anderson in the 1950's. However, none of these authors appeared to take this idea very seriously, or at least to realise just how significant it might be for the future of condensed matter physics in general. Eventually, however, in 1959, the seed was successfully planted; it took root and gave rise to the vast forest of papers on soft mode phase transitions which we now find on the library shelves. The crucial event was the arrival at the Chalk River Nuclear Labs of W. Cochran, in the fall of 1958, to spend a sabbatical leave working with B.N. Brockhouse on the then brand-new subject of lattice dynamics and neutron inelastic scattering. Two breakthroughs of great significance occurred during that year, in connection with Brockhouse's pioneering neutron scattering experiments on Ge and NaI. First was the idea of the shell model of lattice dynamics, which successfully accounted for the major effect of ionic polarizability on the vibrational modes. Leading

on from this success, Cochran saw the significance for ferroelectricity of a steadily decreasing transverse optic mode frequency for q = 0; he developed what has since become known as the soft mode theory, and applied it to the perovskite structure (Cochran 1960).

Convincing demonstrations of the validity of these ideas come a little later with neutron scattering experiments at Chalk River by a student of Cochran, R.A. Cowley. In Fig. 11 we see this first demonstration of soft mode behaviour, in $SrTiO_3$. Cochran's model predicted that the square of the frequency of a particular TO mode would vary linearly with temperature in the same way as does the reciprocal of the dielectric constant as one approaches a ferroelectric phase transition. Over a very wide temperature range, ν_{TO}^2 decreases linearly and would reach zero frequency at $T_c \approx 32$ K if no additional mechanisms came into play. Actually, as you can see from the way $1/\varepsilon$ flattens off as $T \to 0$, the linear behaviour does not hold at very low temperatures and the transition to a ferroelectric phase does not in fact occur at any temperature. Nevertheless, ν_{TO}^2 does follow closely the temperature dependence of $1/\varepsilon$, that is, the Lyddane-Sachs-Teller relation is obeyed, at least down to 4 K, as shown by the solid line in Fig. 12, taken from a 1969 paper by

Yamada and Shirane.

Strontium titanate has provided much food for thought by both experimental and theoretical physicists over at least a decade. Accurate measurements of its unit cell dimensions showed that it becomes very slightly tetragonal below T_a = 108 K and an observed specific heat anomaly confirmed the occurrence of a second-order phase transition at this temperature. However, as indicated in Fig. 11, the dielectric constant shows no anomaly in this region, and it took some years before people realized that this transition involved a particular zone boundary normal mode, at $\underline{q}$ = (0.5, 0.5, 0.5), quite distinct from the q = 0 TO mode associated with the "almost-but-not-quite ferroelectric" transition. In the cubic, paraelectric phase above 108 K, this zone boundary mode is triply degenerate: its temperature dependence as measured by neutron inelastic scattering experiments at Chalk River is shown in Fig. 13. Once again, we see a linear decrease of ν^2 with T, almost but not quite down to the critical temperature T_a. Then the transition to tetragonal antiferroelectric phase occurs, and the mode splits into a doubly degenerate and a single mode, both of which rise in frequency as the temperature is further decreased. The eigenvectors of this Γ_{25} mode correspond to cooperative oxygen ion motions of the form indicated in Fig. 14. In effect, the oxygen octahedra rotate about one of the cube axes, which below T_a becomes the tetragonal axis, so that

rotation in adjacent unit cells are in opposite senses, like a set of interlocking gear wheels. The phase relation π between neighbouring cells is, of course, precisely what we expect for a zone boundary mode.

Many other perovskite crystals have been studied and their structural phase transitions correlated in this way with the temperature dependence of various modes of vibration. In $LaA\ell O_3$, for example, oxygen octahedron rotations are again involved, this time about the cube body diagonal direction, so that the low temperature phase has a trigonal rather than a tetragonal structure. For more comprehensive information, I refer you to several excellent review articles in the Proceedings of the 1971 NATO Advanced Study Institute entitled "Structural Phase Transitions and Soft Modes". A very recent paper on $NaNbO_3$ by Gervais et al. (1982) demonstrates that this kind of soft mode transition is still very much in vogue.

10. Beyond the Simple Soft Mode Concept.

Up to this point I have concentrated almost exclusively on displacive phase transitions, in which a particular mode of vibration of small amplitude tends to zero frequency and the ions become "frozen" in their displaced positions. At the other extreme, there are many examples of order-disorder phase transitions, involving relatively large amplitude atomic movements which take place in a random jump manner at a mean frequency much

lower than the 10^{12} Hz range of typical phonon frequencies. In these cases, such as $NaNO_2$ (Fig. 3), it is physically unreasonable to treat the problem in terms of the phonon (small amplitude) modes. An alternative approach is to introduce a local spin variable $S(\ell s)$ for the atom s in cell ℓ. In the high temperature disordered phase of $NaNO_2$, if a particular N atom is on the left of its O_2, $S = 1/2$, whereas if it is on the right, $S = -1/2$. The dynamics of this "pseudo-spin" system is then treated in exactly the same way as the spin dynamics in a crystal containing magnetic ions with real spins coupled to each other by various kinds of exchange interactions. It is often the case that the spin variable is also coupled to other ionic displacements in the crystal: in $NaNO_2$, for example, the NO_2 dipole direction, denoted by $S(\ell) = \pm 1/2$, strongly influences the neighbouring Na position $u(\ell')$, so that the Hamiltonian for the system should include terms of the form

$\sum_{\ell\ell'} B(\ell\ell')\, S(\ell)\, u(\ell')$. The complications that may arise in treating real crystal transitions which are often intermediate in character between soft mode displacive and the order-disorder types are indeed formidable. A comprehensive discussion of these complications has been given by Cowley (1980).

Interactions of the soft mode with other modes lead to damping of the atomic vibration and hence a broadening of the phonon response. At temperatures well above T_c, the soft mode

frequency is normally much larger than the width or damping constant, $\nu_j(\underline{q}) \gg 2\,\Gamma_j(\underline{q})$. As T falls, however, ν_j eventually becomes comparable to Γ_j and the neutron scattering response from such a mode can be expressed in the quasi-harmonic approximation by a Lorentzian peak of width $2\,\Gamma_i(\underline{q})$, with the δ-function Δ_1 of eq. (4.1) replaced by

$$\frac{\Gamma_j(\underline{q})}{(\nu_j(\underline{q}) \pm \nu)^2 + \Gamma_j^{\,2}(\underline{q})} \qquad (10.1)$$

When $\nu \ll \Gamma$, the response no longer displays a peak near $\pm\,\nu_j(\underline{q})$, but only at $\nu = 0$, and the soft mode is said to be overdamped. This kind of behaviour has been clearly observed in, for example, $BaTiO_3$. The scattering cross section for one-phonon processes involving the overdamped mode can be shown to be approximately proportional to $k_B T/\nu_j^{\,2}(\underline{q})$, so that it diverges as $T \to T_c$ since $\nu_j(\underline{q}) \to 0$. This description of critical scattering, based as it is on the quasi-harmonic approximation, is only a rough qualitative guide to what really happens as T gets very close to T_c.

In fact, in the case of the antiferroelectric transition in $SrTiO_3$, Riste et al. (1971) showed that as T approached T_c from above, at least two distinct contributions to the quasi-elastic neutron scattering were present near the (1/2, 1/2, 3/2) zone boundary point. One component arose from the condensing soft mode becoming overdamped along the lines described

above, while the other was interpreted as being associated with an additional diffusive mode quite distinct from the soft mode. Subsequent experimental studies in many different specimens of $SrTiO_3$ indicated that quasi-elastic scattering could also arise from defects, impurities, or static strain fields, which might have the right symmetry to couple to the condensing soft mode and thus enhance the neutron scattering response. A great deal of interest in tracking down the precise origin of the so-called "central peak" in $SrTiO_3$ and other similar crystals was generated during the early 1970's, and many central peak theories were propounded (see Schwabl 1974, for a review). In the end it seemed that there were at least grains of truth in everyone's theory, and that the central peak did indeed have multiple origins including all those mentioned above.

11. Recent Developments.

As I hinted in an earlier lecture, the soft mode wavevector does not necessarily have to be commensurate with the crystal lattice. An example of this is provided by potassium selenate K_2SeO_4 (Iizumi et al. 1977; Axe et al. 1980), which has an orthorhombic Pnam structure above T_o = 128 K, and undergoes a second-order phase transition to a sinusoidally modulated phase described by a wavevector $\underline{q}_o \approx 0.3\ \underline{a}^*$ where $\underline{a}^*$ is a reciprocal lattice vector. On further cooling to T_c = 93 K, the modulation wavevector changes discontinuously to $\underline{q}_c = (1/3)\underline{a}^*$,

i.e. the structure "locks in" and remains commensurate at all lower temperatures. The new unit cell dimension is 3 times that of the high temperature paraelectric phase.

This low temperature phase is ferroelectric with spontaneous polarization along the c axis. The temperature dependence of the soft phonons propagating along the a* axis in K_2SeO_4 above T_o = 128 K, as determined from neutron inelastic scattering experiments (Iizumi et al. 1977), is shown in Fig. 15. Note that the zone boundary is in the middle of the diagram and the Σ_3 and Σ_2 modes are shown separately in an "extended zone" scheme in the interests of clarity. Clearly the Σ_2 branch near a reduced wavevector $\underline{q}$ = (1/3)a* steadily approaches zero frequency; below 128 K, satellite Bragg reflections appear in both neutron and X-ray diffraction patterns, from the condensation of these soft TO phonons at $\underline{q}_\delta = (1-\delta)a^*/3$. δ is a small, temperature-dependent quantity that decreases smoothly from 0.06 to 0.02 at 93 K, whereupon it abruptly falls to zero. The primary order parameter here is the amplitude of the lattice distortion arising from the Σ_2 mode of wavevector $\underline{q}_\delta$. This mode involves rotational motions of the SeO_4 groups about the b axis coupled to translational motions of both the K ions and SeO_4 groups along c. This information was deduced from measurements of the one-phonon intensities for the same $\underline{q}_\delta$ but in different Brillouin zones, followed by application of eqs. (4.1) and (4.2).

Despite a very considerable amount of experimental and theoretical effort in recent years, it seems that we still do not really understand the physical origin of the incommensurate lattice instability in K_2SeO_4. Considerable progress has been made, however, during which several new concepts, like amplitudons and phasons, have been generated, and an object from the last century called the soliton has been resurrected because of its evident applicability to incommensurate phase transitions. A detailed discussion of these ideas is beyond the scope of these lectures, but in view of their widespread appearance in the recent phase transition literature, a few brief comments may be worthwhile.

In an incommensurate phase, since the wavevector q_δ is not commensurate with the crystal lattice, the order parameter (i.e. the amplitude of the atomic motion which describes the lattice distortion) is a complex number, specified by an amplitude and a phase. Fluctuations in amplitude and phase give rise to new excitations of the crystal, the so-called amplitudons and phasons. The amplitudons are essentially normal optic phonon modes. The dispersion relation for the phasons is believed theoretically to resemble that for acoustic phonons. Indeed, it is hard to see how to distinguish between a phason branch and an acoustic branch emanating from any given satellite Bragg peak, and it is arguable whether there is yet any hard experimental evidence for the existence of phasons (see Cowley 1980).

The phase of $\theta(x)$ of the atomic distortion as we proceed along the x axis of the incommensurate crystal may change in a simple linear manner. An alternative possibility, which may well have lower energy, is that $\theta(x)$ remains constant for a certain distance, then changes smoothly in a relatively short distance to a new value, as sketched in Fig. 16. The region in which $\theta(x)$ changes rapidly has the characteristics of a domain wall separating neighbouring regions of crystal of constant atomic distortion. A soliton is an elementary excitation of these domain walls, which describes their movements through the crystal. The kind of domain wall motion was first observed in 1834 by a Scottish engineer called John Scott Russell. While watching the progress of a barge along a canal, he noted that if the barge stopped suddenly, a wave associated with the bows of the obstructed barge continued on down the canal. Russell was able to observe the progress and properties of this "solitary wave" for many miles down the canal. No doubt he would have been extremely interested as well as amused by the recent rebirth of his solitary wave ideas in connection with incommensurate structural phase transitions.

Bibliography

"Thermal Neutron Scattering", ed. P.A. Egelstaff (1965), New York.

"Theory of Thermal Neutron Scattering", W. Marshall and S.W. Lovesey (1971), Oxford.

"Neutron Spectroscopy and Lattice Dynamics", G. Dolling (1974), in "Dynamical Properties of Solids", eds. G.K. Horton and A.A. Maradudin, North Holland/American Elsevier.

"The Theory and Practice of Neutron Inelastic Scattering", G. Dolling (1975), in Proc. Enrico Fermi School of Physics, Course LV.

"Neutron Diffraction", G.E. Bacon (1975), 3rd edition, Oxford.

"Introduction to the Theory of Thermal Neutron Scattering", G.L. Squires (1978), Cambridge.

References

Axe, J.D., M. Iizumi and G. Shirane (1980), Phys. Rev. B22, 3408.

Brockhouse, B.N. (1961), in "Inelastic scattering of neutrons in solids and liquids" (Int. Atomic Energy Agency, Vienna) p.113.

Cochran, W. (1960), Adv. in Phys. 9, 387.

Cowley, R.A. (1962), Phys. Rev. Lett. 9, 159.

Cowley, R.A., W.J.L. Buyers and G. Dolling (1969), Solid State Commun. 7, 181.

Cowley, R.A. (1980), Adv. in Phys. 29, 1.

Gervais, F., J.L. Servoin, J.F. Banmard and F. Denoyer, (1982) Solid State Commun. 41, 345.

Iizumi, M., J.D. Axe, G. Shirane and K. Shimaoka, (1977) Phys. Rev. B15, 4392.

McMillan, W.J. (1976), Phys. Rev. B14, 1496.

Raman, C.V. and T.M.K. Nedungadi (1940), Nature 145, 147.

Riste, T., E.J. Samuelsen and K. Otnes, (1971), in "Structural phase transitions and soft modes" (Oslo); p. 395.

Schwabl, F. (1974), in "Anharmonic lattices, structural transitions and melting", ed. T. Riste (Noordhoff-Leiden) p. 87.

Van Hove, L. (1954), Phys. Rev. 95, 249.

Yamada, Y. and G. Shirane (1969), J. Phys. Soc. Japan 26, 396.

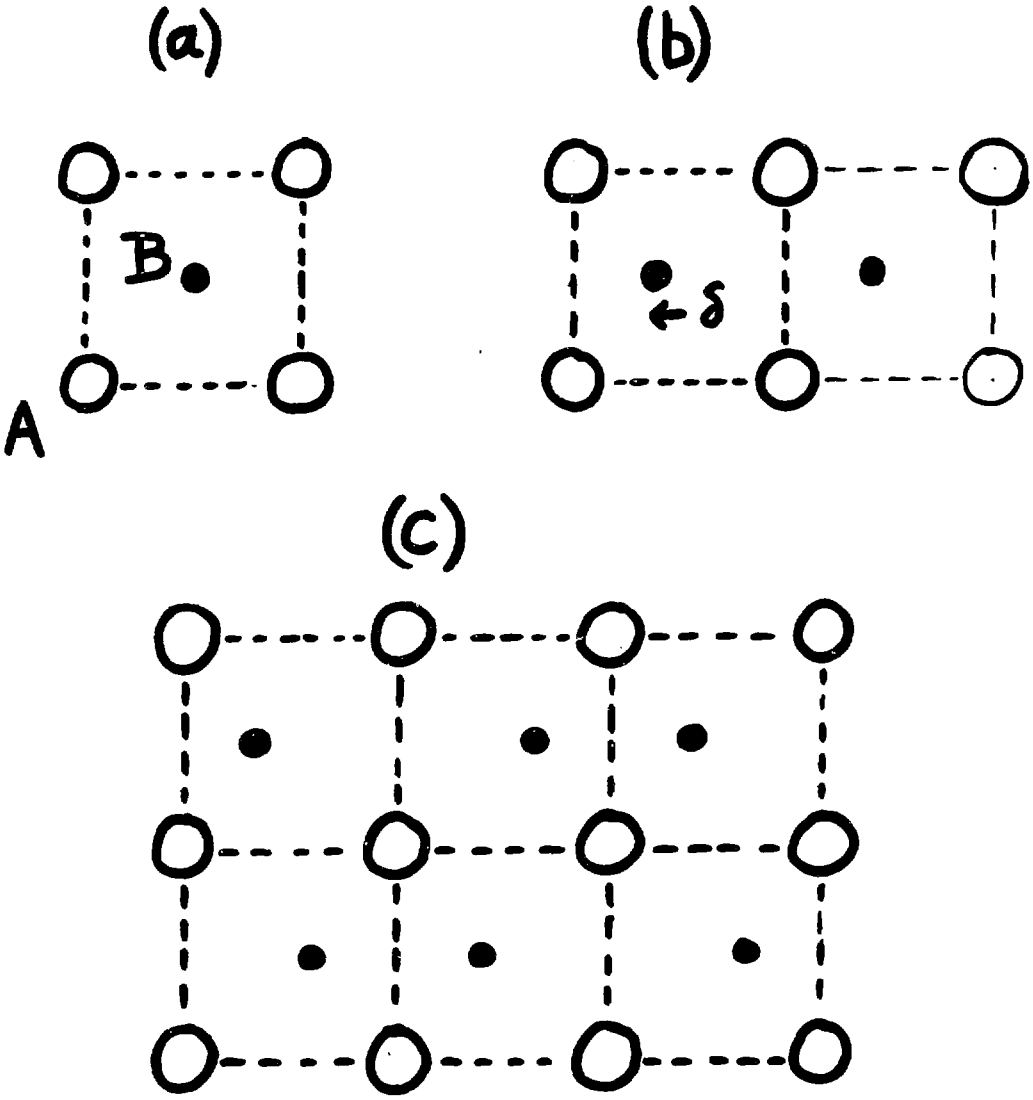

Fig. 1 Two dimensional diatomic crystal AB (a) symmetric square, paraelectric; (b) ferroelectric phase, all ions of type B shifted to the left; (c) antiferroelectric phase B ions shifted alternately left and right in adjacent cells.

POTASSIUM NIOBATE

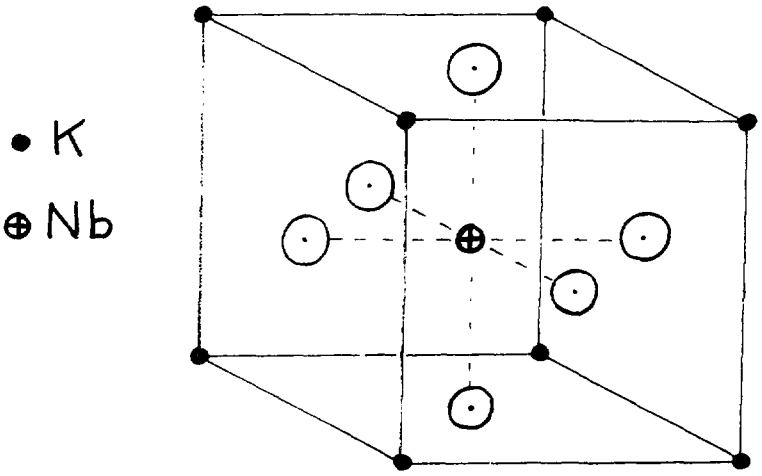

T (K)				
	Cubic	O_h^1	Pm3m	symmetric
708				
	Tetragonal	C_{4v}^1	P4mm	001
488				
	Orthorhombic	C_{2v}^{14}	Amm2	011
233				
	Rhombohedral	C_{3v}^1	P3m1	111

Fig. 2 Three successive ferroelectric phase transitions in $KNbO_3$.

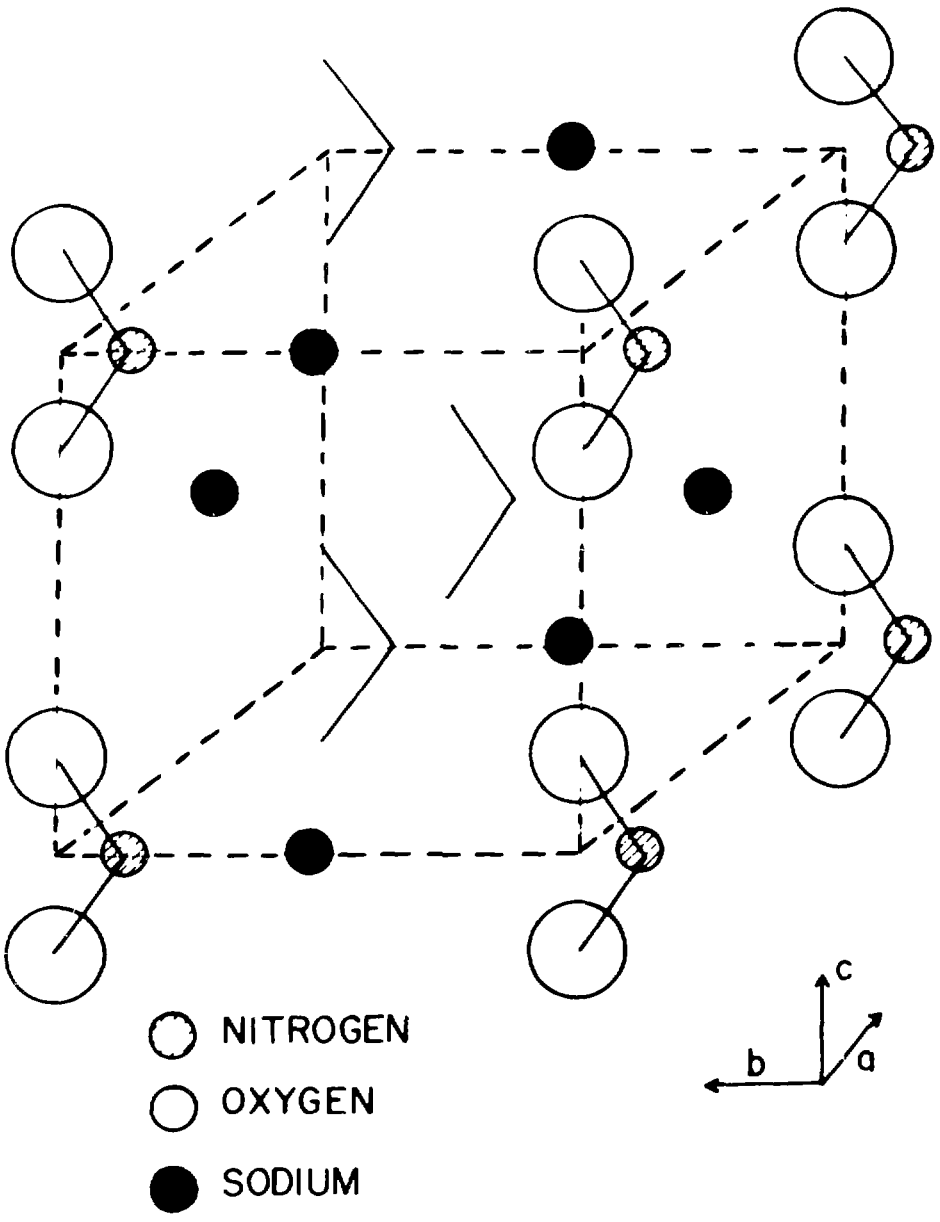

Fig. 3 Ferroelectric structure of $NaNO_2$, below 434 K.

A.E.C.L. Ref. # A-2928-J

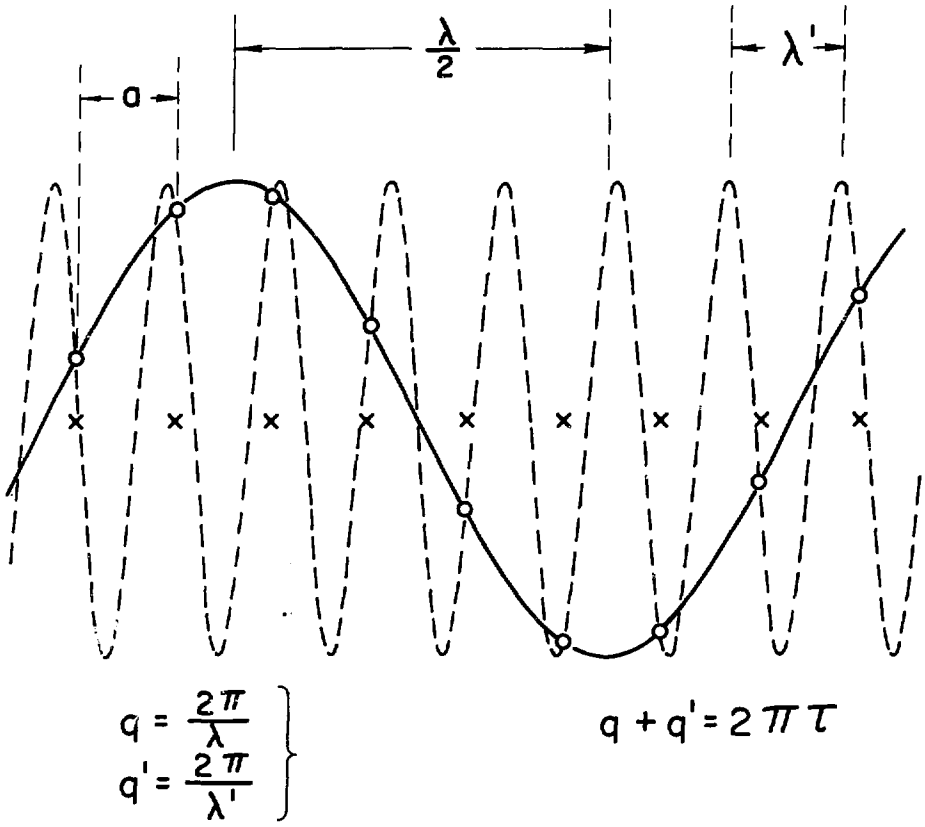

Fig. 4 Equivalence of modes whose wavevectors differ by integer multiples of $2\pi/a$, where a is a unit cell dimension.

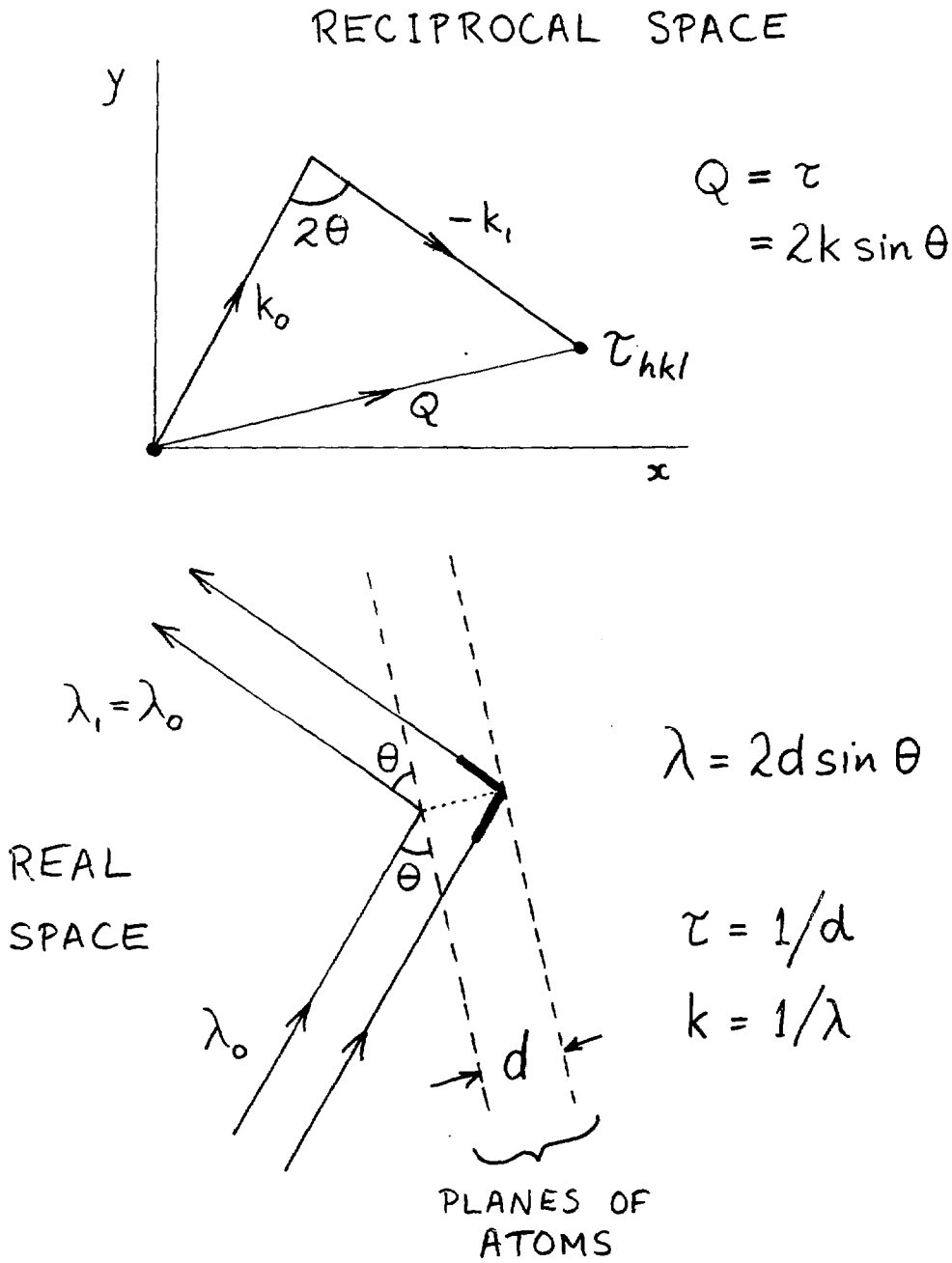

Fig. 5 Illustration of the Bragg law and its representation as a δ-function in momentum space.

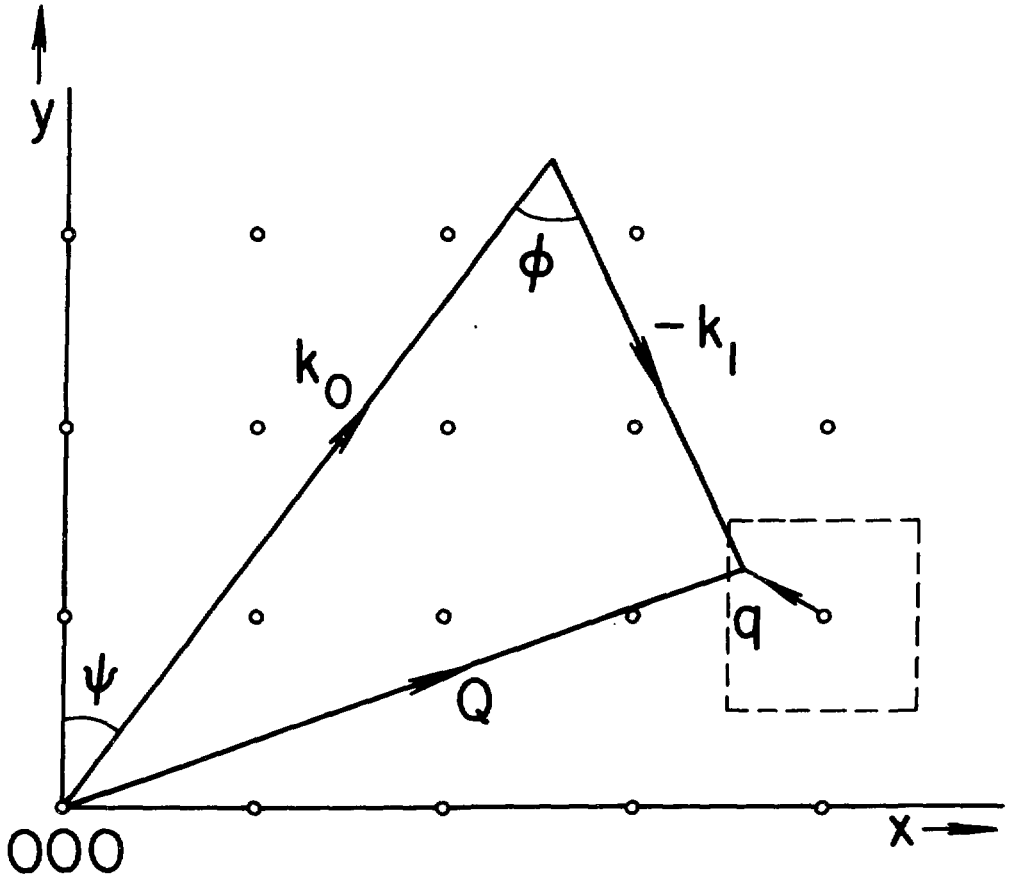

Fig. 6 Reciprocal lattice diagram for a typical crystal. The small circles are reciprocal lattice points in the (xy) plane which contains the incident and scattered neutron wavevector $\underline{k}_0$ and $\underline{k}_1$.

A.E.C.L. Ref. # A-2597-G

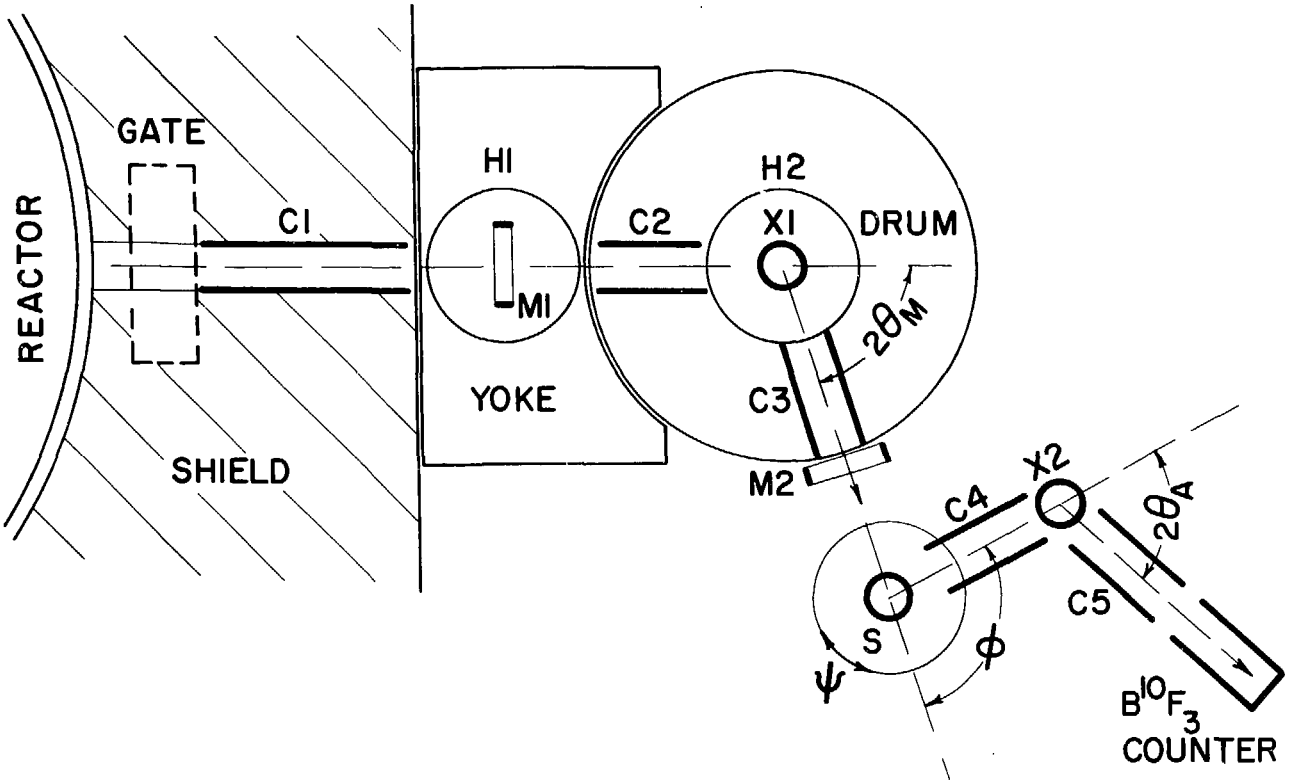

Fig. 7 Schematic diagram of the triple axis crystal spectrometer at the C-5 facility, NRU reactor, Chalk River. C1 - C4 are collimators for defining the direction of the neutron beam as it is scattered in turn by the monochromator crystal X_1, specimen S and analyser crystal X_2. M_1 and M_2 are monitor detectors for the white radiation and the monoenergetic neutron beam, respectively.

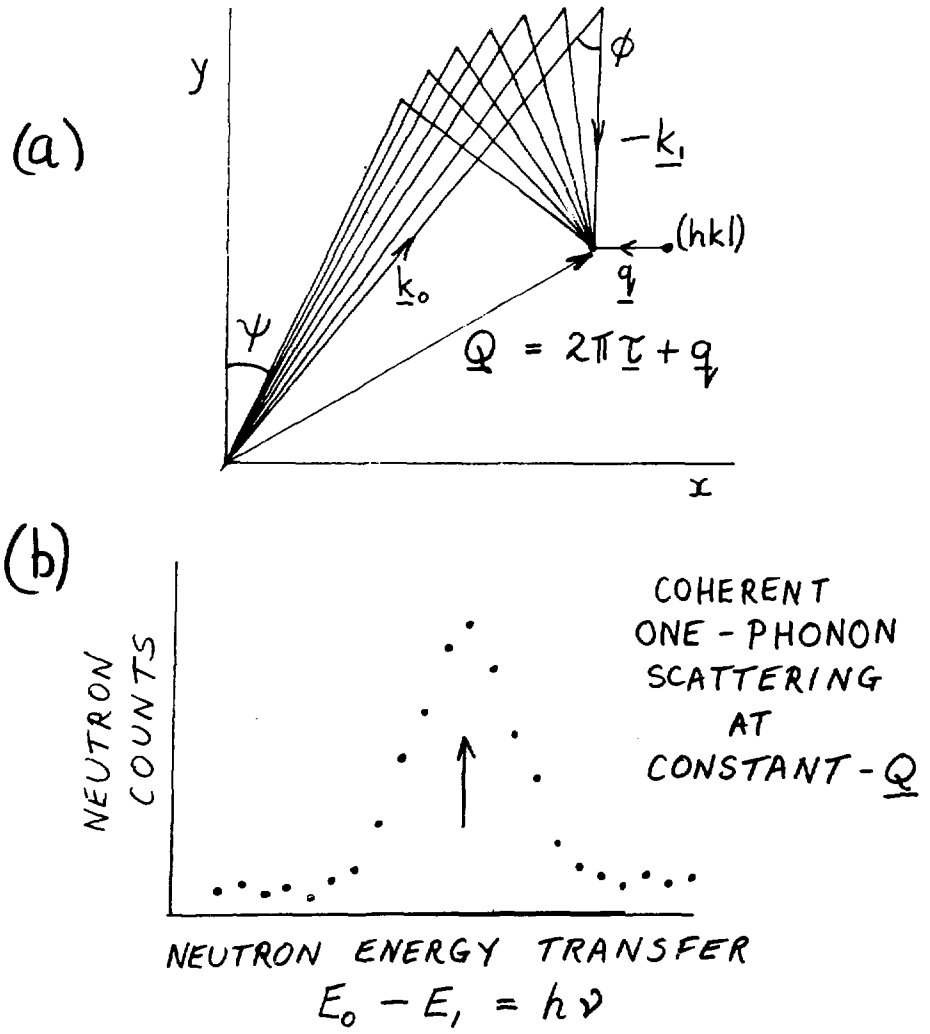

Fig. 8(a) Reciprocal space representation of successive steps in a Constant-Q scan, covering a range of neutron-energy transfer for a fixed value of scattered neutron energy and wavevector magnitude.

(b) Results of the typical scan sketched in Fig. 8(a). Neutron intensity per unit monitor count, as a function of neutron energy transfer.

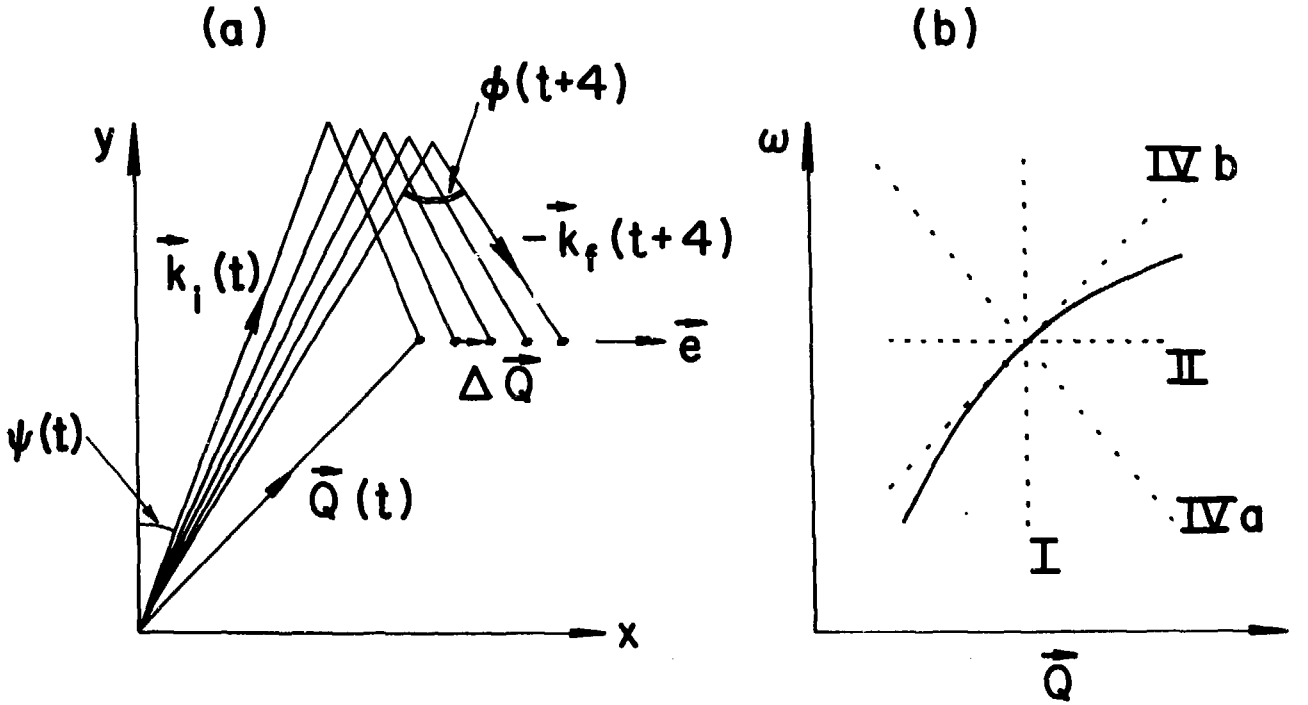

Fig. 9(a) Representation of five successive points on a general linear scan in which ν (or $\omega/2\pi$) and Q change by constant steps.

Fig. 9(b) The dashed straight lines represent some of the possible linear scans illustrated in Fig. 9(a). I and IV are constant-Q and constant energy scans, respectively. The solid line is a typical dispersion curve for excitations in a crystal.

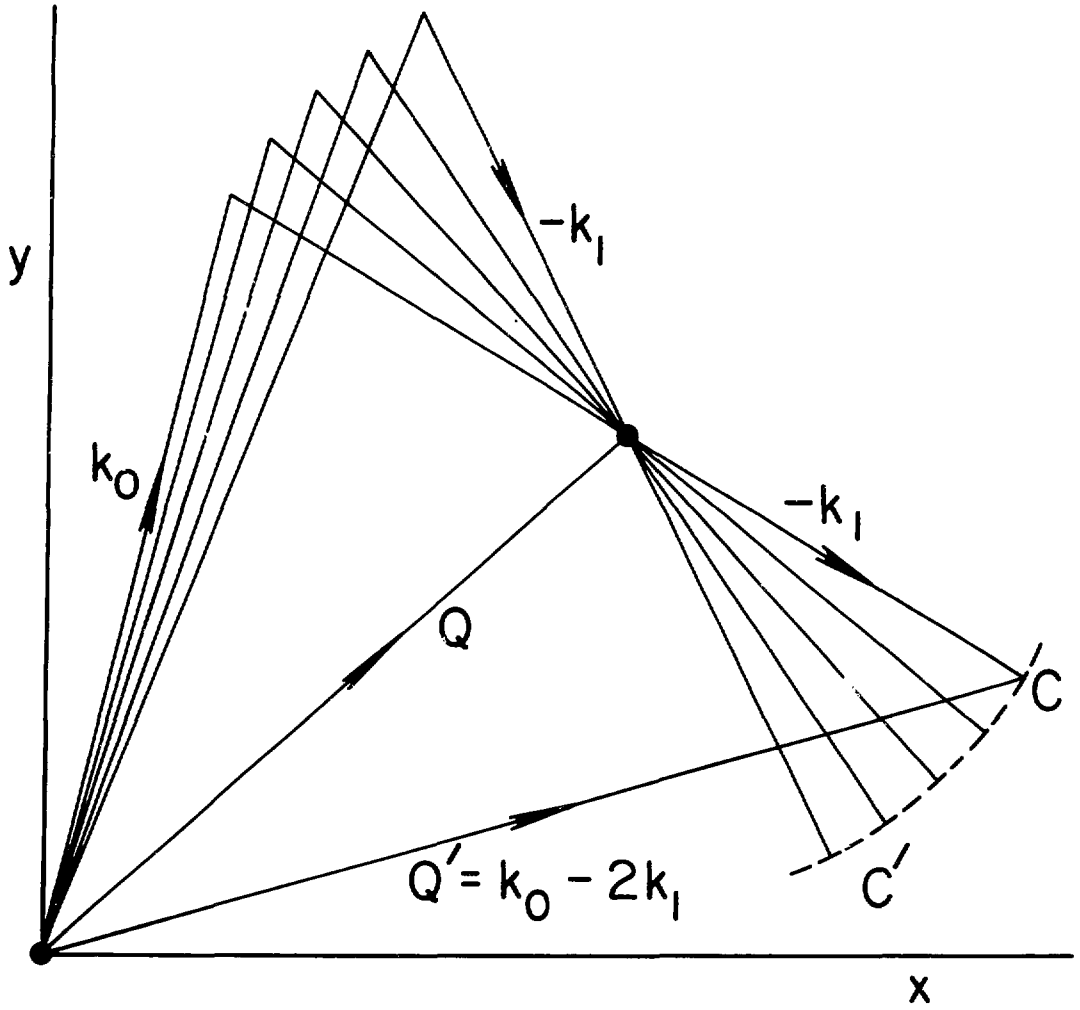

Fig. 10(a) Representation of several successive points on a Constant-$\underline{Q}$ scan, made with an analyser crystal having a significant reflectivity for second-order neutrons of wavevector $2\underline{k}_1$.

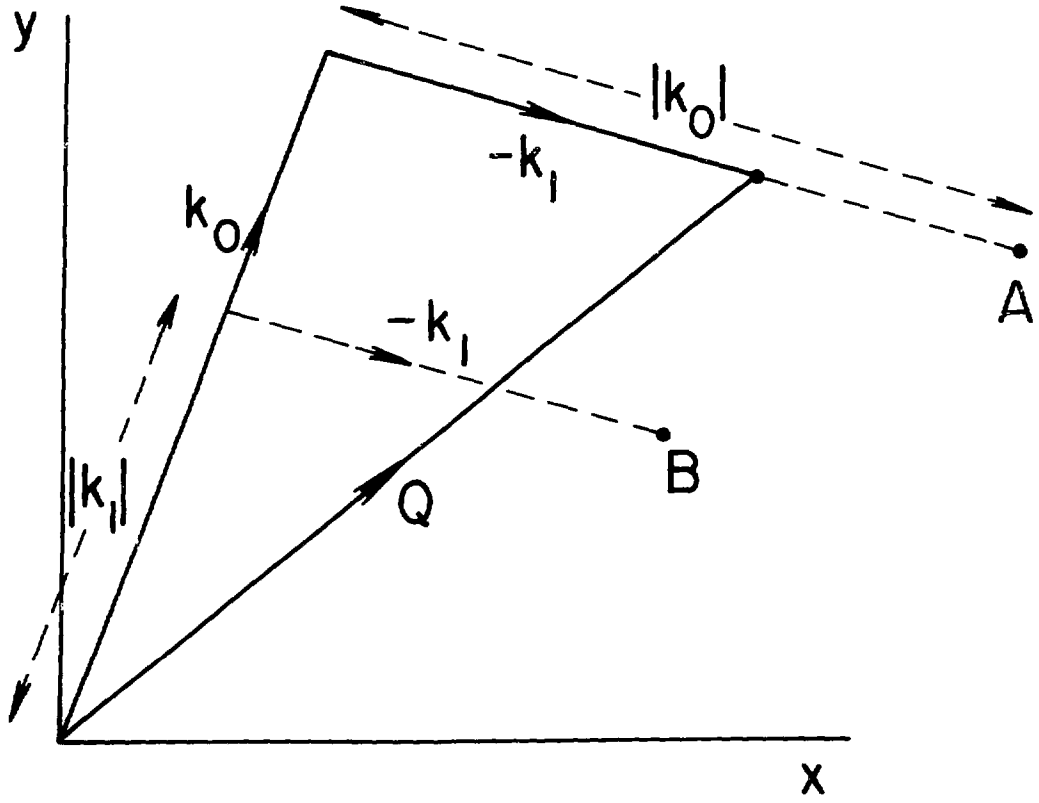

Fig. 10(b) Effect of diffuse scattering from either the monochromator or analyser crystals, coupled with Bragg scattering from the specimen crystal. If either A or B are actual reciprocal lattice points, then a spurious peak may be observed during the scan.

A.E.C.L. Ref. # A-2828-J

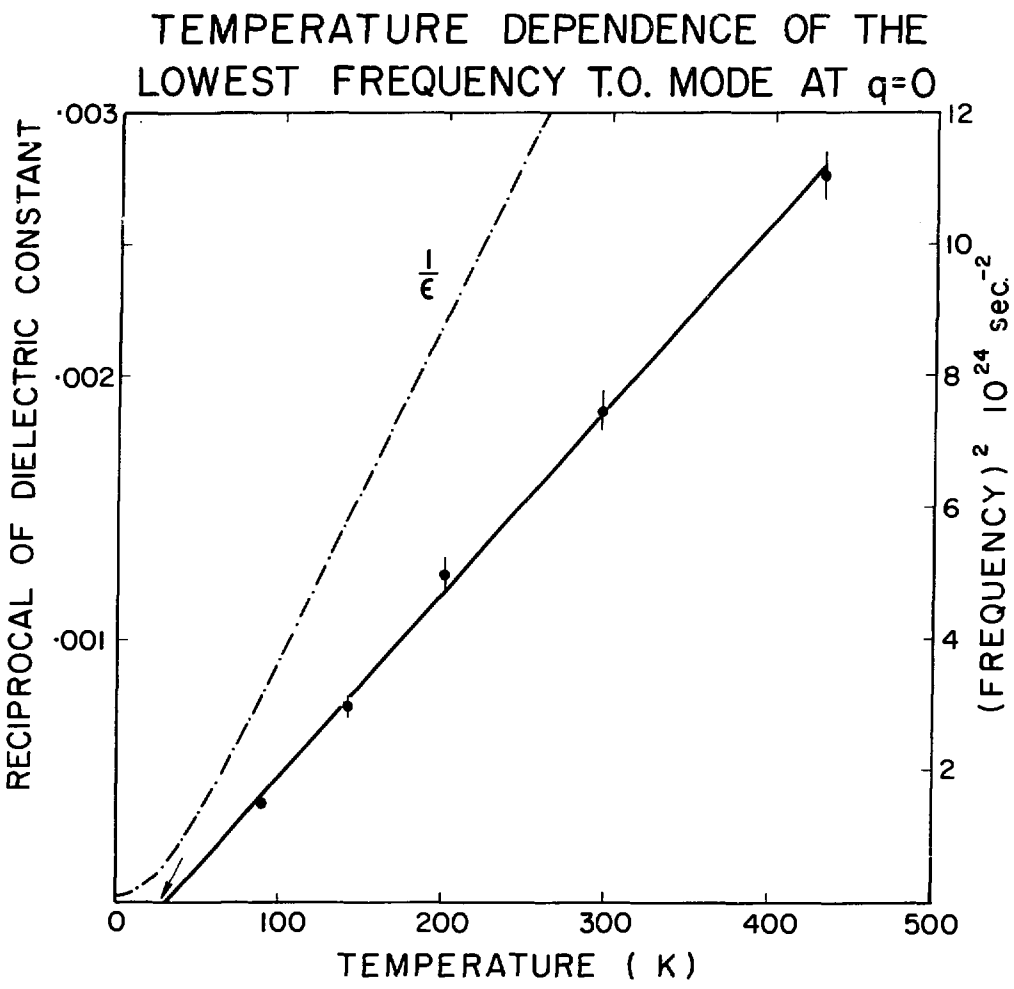

Fig. 11 The square of the frequency of the transverse optic mode of wavevector q = 0 in $SrTiO_3$ as a function of temperature. The dash-dot line gives the reciprocal of the static dielectric constant (Cowley 1962).

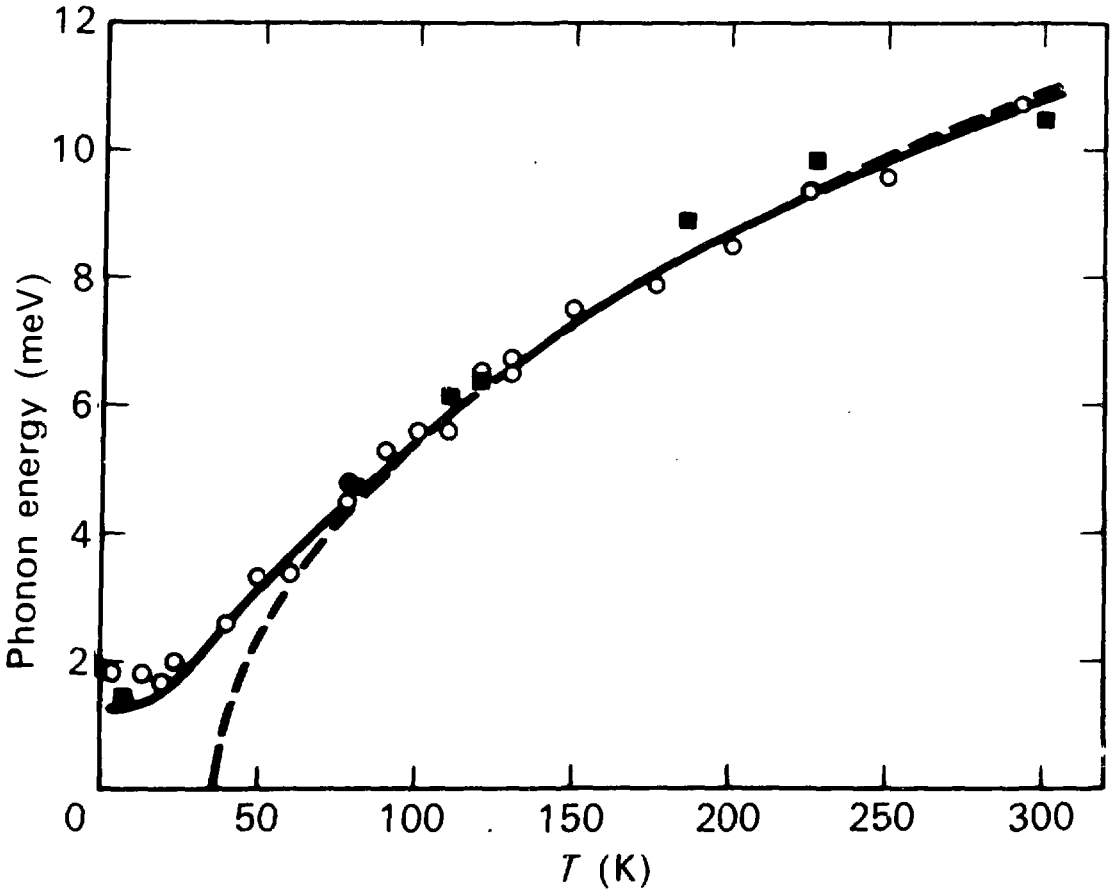

Fig. 12 The energy $h\nu_j(q)$ of the TO mode of $q = 0$ as measured by Yamada and Shirane (1969), down to very low temperatures. The dashed line shows the behaviour of this mode if its frequency ν_j continued to vary as $(T - T_c)^{1/2}$, with $T_c = 32$ K.

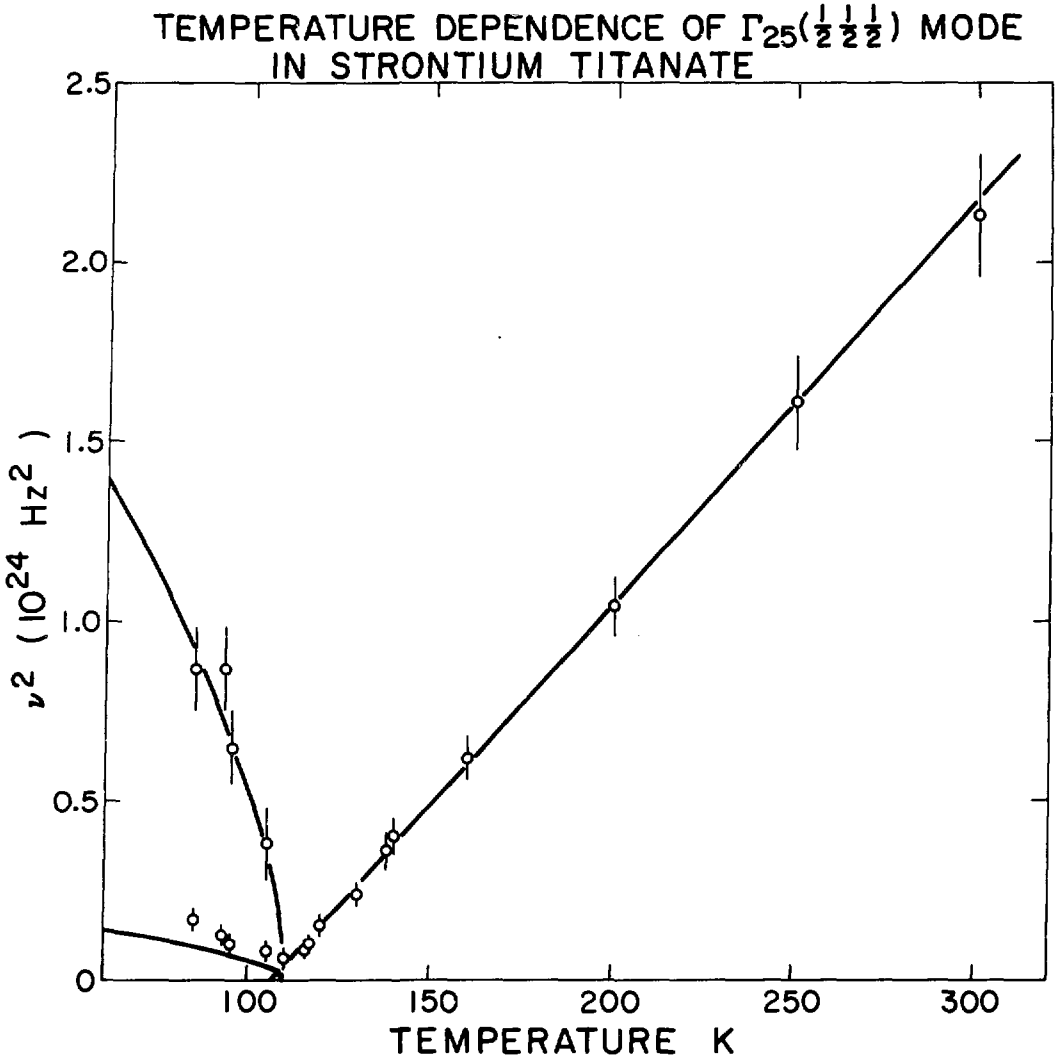

Fig. 13 The square of the frequency of the lowest zone boundary mode, of wavevector (1/2, 1/2, 1/2) and symmetry Γ_{25}, as a function of temperature above the antiferroelectric transition near 108 K. Below this, the lower crystal symmetry (tetragonal) splits this triply degenerate mode into a singlet and a doublet (Cowley et al. 1969).

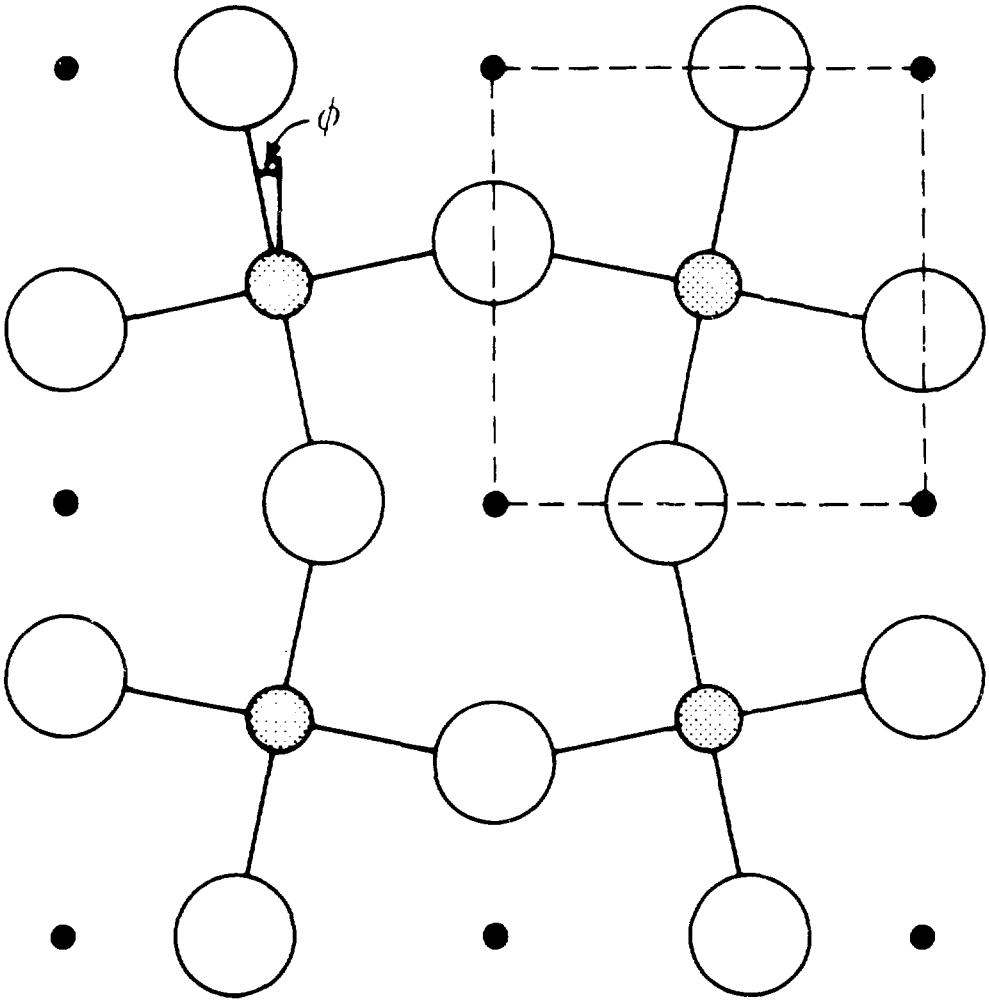

Fig. 14 A section through the structure of $SrTiO_3$ below 108 K, showing the antiphase rotations of the oxygen octahedra. The unit cell of the cubic phase is shown by the dotted lines, and the tetragonal c axis is perpendicular to the plane of the paper.

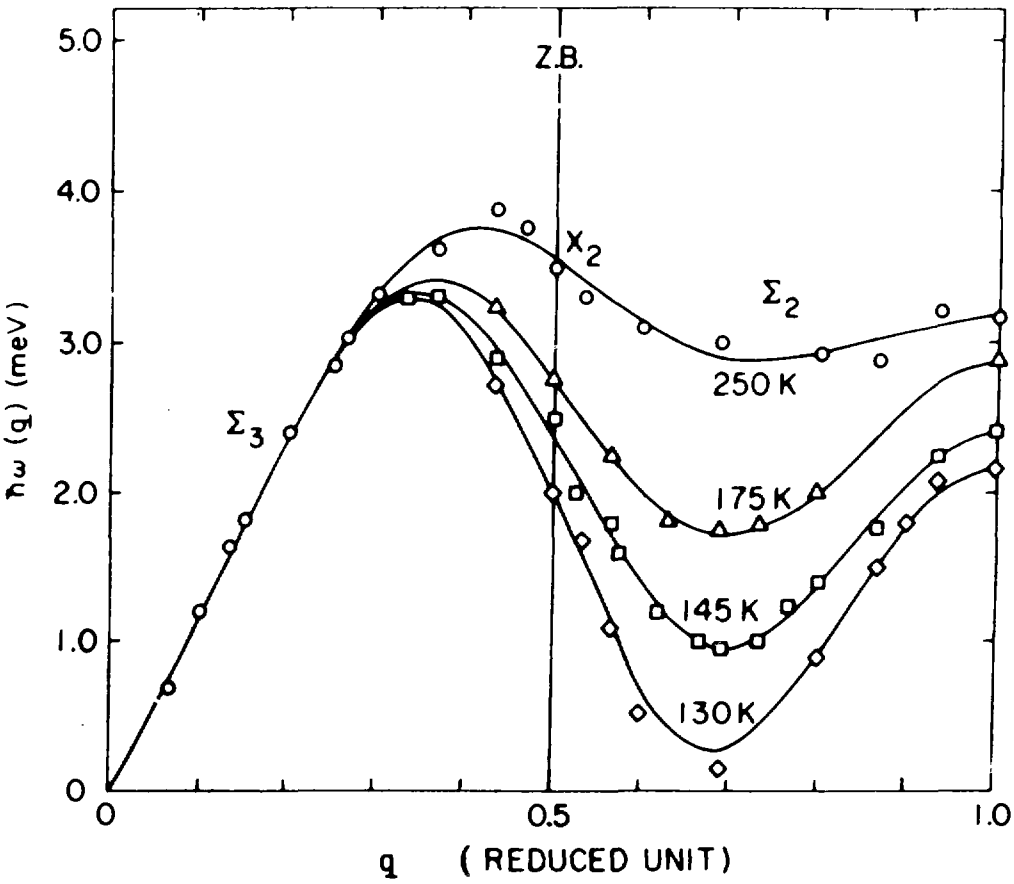

FIg. 15 Dispersion relation of the Σ_2 soft phonon mode in K_2SeO_4 plotted in an extended zone scheme as an extension of the Σ_3 acoustic mode, along the a* direction, as a function of temperature in the paraelectric phase. At 128 K, near $q = 2/3$, the mode reaches zero frequency and a phase transition to an incommensurate structure results (Iizumi et al. 1977). 1 MeV ≡ 0.242 THz and $\omega = 2\pi\nu$.

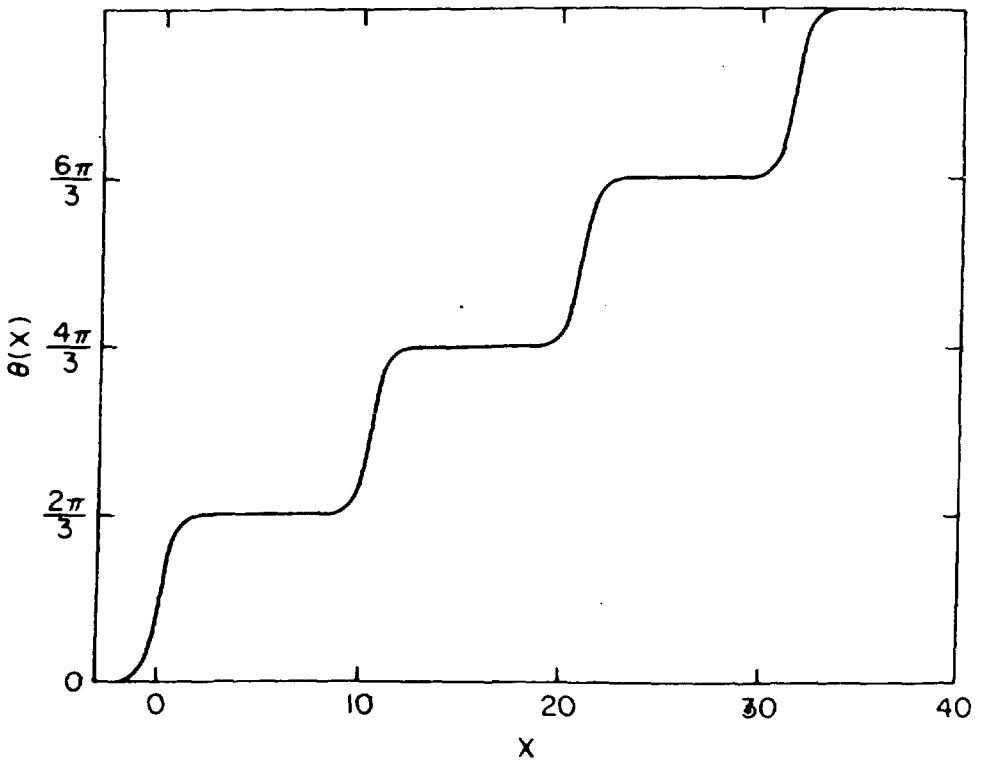

Fig. 16 Variation of the phase function θ(x) close to a "lock-in" transition of the type where the soft mode wavevector is 1/3 of the periodicity of the high temperature paraelectric phase. Instead of displaying an incommensurate wavevector, the phase locks into a commensurate value over certain regions of x, and then switches rather rapidly by 2π/3 in a domain wall region (McMillan 1976).

ISSN 0067 - 0367

To identify individual documents in the series we have assigned an AECL- number to each.

Please refer to the AECL- number when requesting additional copies of this document

from

Scientific Document Distribution Office
Atomic Energy of Canada Limited
Chalk River, Ontario, Canada
K0J 1J0

Price $4.00 per copy

ISSN 0067 - 0367

Pour identifier les rapports individuels faisant partie de cette série nous avons assigné un numéro AECL- à chacun.

Veuillez faire mention du numéro AECL- si vous demandez d'autres exemplaires de ce rapport

au

Service de Distribution des Documents Officiels
L'Energie Atomique du Canada Limitée
Chalk River, Ontario, Canada
K0J 1J0

Prix $4.00 par exemplaire